Clim Dyn (2017) 49:521–545
DOI 10.1007/s00382-016-3356-4

Simulated austral winter response of the Hadley circulation and stationary Rossby wave propagation to a warming climate

Ana C. V. Freitas[1,2] · Jorgen S. Frederiksen[3] · Terence J. O'Kane[4] · Tércio Ambrizzi[1]

Received: 21 January 2016 / Accepted: 7 September 2016 / Published online: 19 September 2016

Abstract Ensemble simulations, using both coupled ocean–atmosphere (AOGCM) and atmosphere only (AGCM) general circulation models, are employed to examine the austral winter response of the Hadley circulation (HC) and stationary Rossby wave propagation (SRW) to a warming climate. Changes in the strength and width of the HC are firstly examined in a set of runs with idealized sea surface temperature (SST) perturbations as boundary conditions in the AGCM. Strong and weak SST gradient experiments (SG and WG, respectively) simulate changes in the HC intensity, whereas narrow (5°S–5°N) and wide (30°S–30°N) SST warming experiments simulate changes in the HC width. To examine the combined impact of changes in the strength and width of the HC upon SRW propagation two AOGCM simulations using different scenarios of increasing carbon dioxide (CO_2) concentrations are employed. We show that, in contrast to a wide SST warming, the atmospheric simulations with a narrow SST warming produce stronger and very zonally extended Rossby wave sources, leading to stronger and eastward shifted troughs and ridges. Simulations with SST anomalies, either in narrow or wide latitude bands only modify the intensity of the troughs and ridges. SST anomalies outside the narrow latitude band of 5°S–5°N do not significantly affect the spatial pattern of SRW propagation. AOGCM simulations with 1 %/year increasing CO_2 concentrations or 4 times preindustrial CO_2 levels reveal very similar SRW responses to the atmospheric only simulations with anomalously wider SST warming. Our results suggest that in a warmer climate, the changes in the strength and width of the HC act in concert to significantly alter SRW sources and propagation characteristics.

Keywords Hadley circulation · Atmospheric simulations · Coupled simulations · Stationary Rossby wave

1 Introduction

The Hadley cell (HC) is generally defined as the zonal mean meridional mass circulation in the atmosphere, with warmer air rising in the tropics and colder air sinking in the subtropics. This thermally driven meridional circulation extends roughly between 30°S and 30°N and plays a key role in the climate system by transporting momentum and heat from the tropics to the subtropics (Lindzen 1994).

There has been a recent and growing interest in studying the Hadley circulation changes in response to global climate change. Most studies have focused on the alterations in HC strength and width with the objective of verifying how these changes affect the regional and global climates. An observational study by Johanson and Fu (2009) showed that the HC has widened by about 2°–5° since 1979 and that this observed widening cannot be explained by natural variability. This widening and the concomitant poleward displacement of the subtropical dry zones may be accompanied by large-scale drying near 30°N and 30°S. Idealized and comprehensive general circulation models (GCMs) have also shown HC widening in response to increases in greenhouse gases and changes in the thermal structure of the polar

✉ Ana C. V. Freitas
ana.freitas@unifei.edu.br

[1] Institute of Astronomy, Geophysics and Atmospheric Sciences (IAG), University of São Paulo (USP), São Paulo, SP, Brazil

[2] Federal University of Itajubá/UNIFEI, Itabira, MG, Brazil

[3] CSIRO Oceans and Atmosphere, Aspendale, VIC, Australia

[4] CSIRO Oceans and Atmosphere, Hobart, TAS, Australia

stratosphere (Polvani and Kushner 2002; Lu et al. 2007; Frierson et al. 2007).

Lu et al. (2008) tested the hypothesis that the circulation response to global warming might resemble the circulation response to El Niño. The authors found different HC responses to global warming and to El Niño events. Global warming produces expansion and weakening of the HC, while El Niño produces contraction and strengthening of the HC. Also, global warming produces a poleward shift of the mid-latitude jets, while El Niño produces an equatorward shift. This contrast is intriguing because both El Niño and global warming produce substantial warming of the tropical troposphere. Tandon et al. (2013) studied this issue and found that a thermal forcing applied to a narrow region around the equator produces ''El Niño–like'' HC contraction and equatorward shift of the jets, while a forcing with wider meridional extent produces ''global warming–like'' HC expansion and poleward shift of the jets. Thus, this means that seemingly subtle alterations to the meridional structure of a thermal forcing can have a dramatic effect on the circulation response.

Frierson et al. (2007) showed that the width of the HC responds similarly to changes in sea surface temperature (SST) distribution in idealized and full GCMs: both models respond with a widening of the HC in response to increases in global mean temperature, and, to a lesser extent, to increases in meridional temperature gradients. Increases in SST and SST gradients lead to increases in the dry static stability, which then reduces baroclinic growth rates and pushes the latitude of baroclinic instability onset (and therefore the edge of the HC) to a location that is farther poleward. The authors also found that the HC width increases within an idealized moist GCM were similar to those with a comprehensive GCM; this suggests that HC width does not strongly depend on model physics. Gastineau et al. (2009) investigated the role played by the detailed structure of the SST change on the large-scale atmospheric circulation. The authors clearly demonstrated that changes in the zonal-mean meridional gradients of SST are the main modulators of the HC strength, whereas the winter hemisphere HC poleward expansion was well captured by the simulations with a globally uniform SST warming, without any latitudinal or longitudinal changes in SST gradients.

The studies mentioned above focused on the investigation of HC changes and what drives them. However, there are few studies examining how these changes in the strength and width of the HC affect the extra-tropical atmospheric circulation. The tropical variability is connected with the extra-tropical atmospheric circulation through teleconnections induced by Rossby-wave dynamics, with important implications for regional climates by modifying patterns of temperature and precipitation. Many of the observed teleconnection patterns in the atmosphere can be explained by a disturbance in the vorticity field caused by the tropical deep convection in the ascending branch of the HC, associated with anomalous divergence at high levels. This triggers large-scale atmospheric Rossby waves, which can propagate into higher latitudes along a ray path (Hoskins and Karoly 1981; Hoskins and Ambrizzi 1993). Thus, local forcing in specific places can influence remote regions through organized structures in the form of waves, and one way to analyse this wave propagation is using stationary Rossby wave linear theory in a barotropic atmosphere (Müller and Ambrizzi 2007; Müller and Berri 2007).

Freitas and Ambrizzi (2012) found observationally, for the austral winter, that weak HC years are characterized by a wave train with zonal wavenumber three, trapped inside the polar jet waveguide, emanating from the subtropical central-west Indian Ocean in an arc-like route and reaching the north of South America. On the other hand, strong HC years are characterized by a wave train with zonal wavenumber four, also trapped inside the polar jet waveguide, emanating from subtropical central-east Indian Ocean and reaching the subtropical west coast of Africa. The authors showed that over South America the HC weakening can lead to a very cold and rainy winter in the southwest of the continent and a mild warm and dry winter in the Brazilian states of Minas Gerais and Bahia. An almost opposite configuration is seen with the HC strengthening.

Several studies have shown the important role of tropical SST anomalies and external radiative forcing in driving changes in local and/or remote atmospheric circulation through the propagation of planetary waves from regions of anomalous upper-level divergence. For example, Taschetto and Ambrizzi (2012) found a link between the Indian Ocean basin-wide warming and South American climate that occurs via alterations of the Walker circulation pattern and through a mid-latitude wave-train teleconnection. O'Kane et al. (2015), recently applied non-stationary non-parametric multiscale cluster analysis to examine the respective roles of potential vorticity sources, Rossby wave dynamics and baroclinic instability on atmospheric teleconnections in the Southern Hemisphere over the past 60 years. They found significant Rossby wave sources dominated by local processes, and largely contained in the waveguides of the troposphere, exhibiting large secular trends in response to systematic changes in radiative forcing, predominantly carbon dioxide (CO_2).

The aim of this paper is to investigate how simulated changes in the strength and width of the austral winter HC impact upon the extra-tropical planetary waves and their propagation. We set up six ensembles of atmospheric simulations using the CSIRO Mk3L GCM (Phipps 2010), using a set of idealized SST perturbations constructed from

observed SSTs, in order to simulate changes in the strength and width of the HC. In addition, two ensembles of coupled model simulations were set up for a global warming scenario.

Caballero (2007) found that the interannual variability in the strength of the HC is largely associated with extra-tropical eddy stresses. Thus, one could argue about the influence of the midlatitude eddies on the HC; here we will not consider this two-way interaction. Moreover, Kang and Polvani (2011) demonstrated that the summer Hadley cell is more akin to the eddy-driven Ferrel cell, whereas the winter Hadley cell is relatively unaffected by midlatitude eddies. Freitas et al. (2015) showed that atmospheric simulations by the CSIRO Mk3L with observed SSTs and historical time-evolving CO_2 concentrations are quite skilful in reproducing important inter-decadal changes found in the jet streams, temperature, HC, mean sea level pressure and precipitation.

Details of the model and the observational datasets are given in Sect. 2. In Sect. 3, we describe our methodology and show how we set up ensemble atmospheric and coupled simulations which are able to mimic changes in the HC strength and width. In Sect. 4, we firstly analyse the skill of atmospheric simulations; then, in Sect. 5 we investigate separately how simulated changes in the strength and width of the austral winter HC affect the extra-tropical planetary waves. The impact of simulated changes in both the strength and width of the HC upon these waves are examined through coupled simulations in Sect. 6. Finally, discussion and conclusions highlighting the main results of the paper are presented in Sect. 7.

2 Observational datasets and model details

2.1 Reanalysis dataset

The monthly data of zonal and meridional winds used here have been obtained from the the National Centers for Environmental Prediction-Department of Energy (NCEP-DOE) Reanalysis 2[1] (Kanamitsu et al. 2002) on a 2.5° latitude by 2.5° longitude grid at 17 pressure levels. The reanalysis dataset is used to verify how accurately the model simulates the observed HC and the Rossby wave sources.

2.2 Model details

The CSIRO Mk3L GCM version 1.2, designed for the study of climate variability and change on monthly to millennial timescales, is used in this study (Phipps 2010; Phipps et al. 2011, 2013).

2.2.1 Atmosphere model

The atmospheric component of Mk3L is based on the CSIRO Mk3 model (Gordon et al. 2002) with rhomboidal 21 resolution, consisting of equations for atmospheric transport, radiative exchange, convection and clouds. A cumulus convection scheme (Gregory and Rowntree 1990) and a prognostic stratiform cloud scheme (Rotstayn 1997, 1998, 2000) are incorporated in the model. The radiation scheme treats solar (shortwave) and terrestrial (longwave) radiation independently, and includes the effects of CO_2, ozone, water vapour and clouds. The Atmospheric Model Intercomparison Project (AMIP II) recommended dataset (Wang et al. 1995) provides the climatological values for the ozone concentrations.

A hybrid vertical coordinate is used, with 18 vertical levels. Time integration is by a semi-implicit leapfrog scheme, with a Robert-Asselin time filter (Robert 1966), used to prevent decoupling of the time-integrated solutions at odd and even timesteps. The Mk3L atmosphere model uses a timestep of 20 min.

A multi-layer dynamic-thermodynamic sea ice model and a land surface model are included. The temperatures of the sea gridpoints are determined by the monthly-mean observed SSTs for the stand-alone atmosphere model. Linear interpolation in time is used to estimate values at each timestep, with no allowance for diurnal variation.

2.2.2 Coupled model

The coupling between the atmosphere model (AGCM) and ocean model (OGCM) is described in detail by Phipps (2006), and rigorously conserves heat and freshwater. Within the coupled model, four fields are passed from the AGCM to the OGCM: the surface heat flux, surface salinity tendency, and the zonal and meridional components of the surface momentum flux. Four fields are also passed from the OGCM to the AGCM: the SST, sea surface salinity (SSS), and the zonal and meridional components of the surface velocity.

The Mk3L coupled model runs in asynchronous mode, with one OGCM timestep (1 h) being followed by three AGCM timesteps (3 × 20 min). The surface fluxes calculated by the AGCM are averaged over the three consecutive AGCM timesteps, before being passed to the ocean model. Bilinear interpolation is used to interpolate the AGCM fields to the spatial resolution of the OGCM. In the case of the surface fields passed from the OGCM to the AGCM, instantaneous values for the zonal and meridional components of the surface velocity are passed to the AGCM. These velocities act as the bottom boundary condition in

[1] NCEP-DOE Reanalysis 2 is available on: http://www.esrl.noaa.gov/psd/data/gridded/data.ncep.reanalysis2.html.

the sea ice model for the following three AGCM timesteps. In the case of the SST and SSS, however, the OGCM passes two copies of each field: one containing the values at the current OGCM timestep, and one containing the values which have been predicted for the next OGCM timestep. The AGCM then uses linear interpolation in time to estimate the SST and SSS at each AGCM timestep. Area averaging is used to interpolate the OGCM fields to the spatial resolution of the AGCM.

Flux adjustments can be applied to each of the fluxes passed from the AGCM to the OGCM, and also to the SST and SSS. Any need to apply adjustments to the surface velocities is avoided by using climatological values, diagnosed from a long OGCM reference simulation, to spin up the AGCM.

3 General methodology

3.1 Definition of HC

A conventional way to depict the HC is to use the mean meridional mass streamfunction ψ (Oort and Yienger 1996), which quantifies air mass transport in the tropics and subtropics. It is computed using the zonal-mean meridional wind and the surface pressure according to the following equation:

$$\psi(\phi, p) = \frac{2\pi a \cos\phi}{g} \int_{p}^{p_s} \left[\overline{v}(p', \phi)\right] dp' \quad (1)$$

Here a is the earth's radius, ϕ is the latitude, $\overline{v}$ is the zonally averaged temporal mean of the meridional velocity, p is the pressure, p_s is the surface pressure, and g is the acceleration of gravity.

A clockwise circulation (as in the NH winter cell) corresponds to a positive value of ψ, whereas a counter-clockwise circulation (as in the SH winter cell) is associated with a negative ψ (Oort and Yienger 1996). Thus, a strengthening (weakening) of the HC corresponds to a negative (positive) value of ψ for the difference between the perturbed and the reference ensemble in JJA (June–July–August).

The strength or intensity of the HC is defined by the maximum value of the zonal mean meridional mass streamfunction. The HC extent is defined using the latitude at which the streamfunction takes the value zero, interpolated on the latitude grid, at the pressure level of 500 hPa (Gastineau et al. 2008; Lu et al. 2007). For JJA, the streamfunction takes the value zero at three points between 45°N and 45°S: two at the extratropical edges of the Northern and Southern Hemisphere cells, and one between the two cells (Gastineau et al. 2008).

3.2 Rossby wave source

Sardeshmukh and Hoskins (1988) studied the generation of Rossby wave trains by the divergent flow in the upper-troposphere from deep tropical convection. They defined the Rossby wave source (RWS), from the barotropic vorticity equation, as:

$$RWS = -\zeta D - \overrightarrow{V_\chi} \cdot \nabla\zeta = -\nabla \cdot (\overrightarrow{V_\chi}\zeta) \quad (2)$$

Here $\zeta = \xi + f$ is the absolute vorticity, ξ is the relative vorticity, f is the Coriolis parameter, $\overrightarrow{V_\chi}$ is the divergent component of the wind velocity field and D is the horizontal divergence $\partial u/\partial x + \partial v/\partial y$. The first component $(-\zeta D)$ is the vortex stretching term (hereafter VS), or the generation of vorticity by divergence, and the second component $(-\overrightarrow{V_\chi}.\nabla\zeta)$ is the advection of absolute vorticity by divergent flow (hereafter AV).

Here we applied a similar analysis method to that of Tyrrell and Karoly (1996), employing maps of divergence, RWS components, and streamfunction, with the aim to identify local HCs, which form direct links between the regions of tropical convection and regions of enhanced Rossby wave forcing in the extratropics.

3.3 CSIRO Mk3L atmosphere model simulations

A set of 6 ensembles have been conducted. Each ensemble of atmospheric simulations has five members, which are constructed by perturbing the initial conditions. The first ensemble or the atmosphere-model reference simulations are forced by the observed monthly mean Hadley Centre Global Sea Ice and Sea Surface Temperature (HADISST) dataset (Rayner et al. 2003)[2] from 1871 to 2010 and historical time-evolving CO_2 concentrations.

We examine separately the impact of changes in the HC strength and width upon the stationary Rossby wave propagation using different SST forcing patterns constructed from the observed SSTs. Thus, in the following subsections we describe the perturbed atmospheric simulations performed as in the atmosphere-model reference simulations, but with a specified spatial component of the SST forcing pattern added to the observed SSTs. The Southern Hemisphere (SH) JJA climate fields in the period 1979–2010 are analysed for the difference between each perturbed ensemble mean and the atmosphere-model reference ensemble mean.

3.3.1 Simulating changes in the HC strength

Gastineau et al. (2009) clearly demonstrated that changes in the zonal-mean meridional gradients of SST are the main modulators of the HC strength. They showed that an increased (decreased) gradient led to an intensified

[2] HADISST dataset is available on: http://www.metoffice.gov.uk/hadobs/hadisst/data/download.html.

(weakened) HC, independent of any change in global mean temperature. The warmer climate by itself actually led to a small decrease in HC intensity (Rind and Perlwitz 2005). Changes in the latitudinal gradient did not affect the width of the HC. Thus, to simulate changes in the HC strength and in order to investigate the effects upon the stationary Rossby wave propagation, strong and weak meridional SST gradients are prescribed in the model.

Here, to either increase or decrease the meridional SST gradient, a continuous and smooth Gaussian function (*GSST*) defined by Vidyunmala et al. (2007) as follows, is applied in the model:

$$GSST\left(^{\circ}C\right) = T_{\max}\left[\exp\left(-\alpha\left[\frac{\phi-\phi_0}{90}\right]^2\right)\right] \quad (3)$$

where α is a measure of the SST gradient, ϕ is the latitude in degrees, ϕ_0 is the latitude of SST maximum, and T_{max} is the maximum SST for the period 1979–2010, which is equal to 28.25 °C. The strong (weak) meridional SST gradient applied here corresponds to $\alpha = 10$ ($\alpha = 1$). Note that the SST gradient is altered when α is changed without changing the SST maximum (Vidyunmala et al. 2007).

The Gaussian curve is then blended with the observed SST field, according to the following equation:

$$SST = (2 \times OSST + GSST)/3 \quad (4)$$

Here *OSST* is the observed SST, i.e. the original time-evolving monthly mean HADISST dataset from 1871 to 2010, and *GSST* is the Gaussian curve obtained from the Eq. (3). The atmospheric simulations with strong (weak) meridional SST gradient prescribed are denoted SG (WG).

Table 1 Description of the atmosphere-model simulations used for the impacts analysis of changes in the HC strength upon the stationary Rossby wave propagation

Simulations	Description
Atmosphere-model reference	Integrated for 140 years from 1871 to 2010 with time-evolving CO_2 concentration and observed SSTs (5-member ensemble)
WG	Integrated for 140 years from 1871 to 2010 with time-evolving CO_2 concentration and weak SST meridional gradient added to the observed SSTs (5-member ensemble)
SG	Integrated for 140 years from 1871 to 2010 with time-evolving CO_2 concentration and strong SST meridional gradient added to the observed SSTs (5-member ensemble)

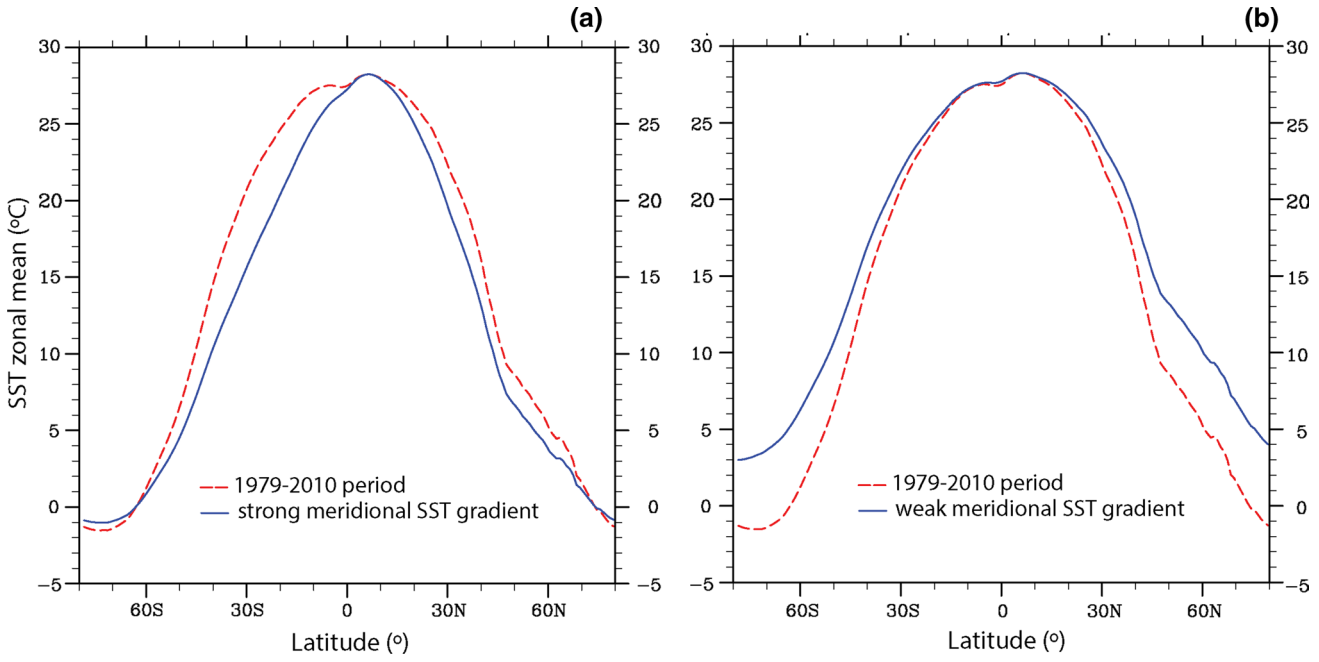

Fig. 1 Zonally averaged observed SST (°C) for the period 1979–2010 (*red dashed line*) and the idealized SST (°C) profiles (*blue solid line*) for (**a**) strong and (**b**) weak meridional SST gradient

The reader is referred to Table 1 for a summary of the ensembles considered here. As well, Fig. 1 shows the zonally averaged observed SST and the idealized profiles for strong ($\alpha = 10$) and weak ($\alpha = 1$) meridional SST gradient for the period 1979-2010. The value of α that best matches the observed SST field is 5.

3.3.2 Simulating changes in the HC width

Tandon et al. (2013), using an idealized GCM, verified that a thermal forcing applied to a narrow region around the equator produced HC contraction and equatorward shift of the jets, while a forcing with wider meridional extent produced HC expansion and poleward shift of the jets. Thus, to simulate changes in the HC width, in order to investigate the effects upon the stationary Rossby wave propagation, we use essentially two different patterns of SST warming.

The warmest anomaly, according to the annually averaged time series of the global SST anomalies (°C) for the HADISST dataset from 1871 to 2010, is around 0.4 °C in the year 1998. As well, the linear trend for the time series of the global and tropical (30°S–30°N) SST anomalies is around 0.4 °C per century, which is statistically significant at the 5 % probability level. Thus, to simulate changes in the HC width, we have prescribed a tropical heating (TH) of 2 °C, which is equal to five times the linear trend per century and the warmest anomaly from 1871 to 2010.

Specifically, to simulate a HC contraction, the TH of 2 °C is applied only from 5°S to 5°N, whereas to simulate a HC expansion it is applied from 30°S to 30°N; leaving unchanged the observed SST field in the other latitudinal bands. The atmospheric simulations for HC contraction (expansion) are denoted TH5 (TH30).

For comparison purposes, another set of experiments is performed by prescribing a SST forcing pattern based on the observed global SST anomalies from the HADISST dataset for the period 1871–2010. To perform this, the calculated monthly observed SST anomalies (at each gridpoint), for each one of the 140 years, were added on top of the original time-evolving monthly mean HADISST dataset at the same latitude bands of the TH30 and TH5 ensembles; thus doubling the anthropogenic signal present in these regions in the original time series. These simulations are denoted ANOM30 and ANOM5, respectively. Table 2 summarizes the atmospheric simulations considered here.

3.4 CSIRO Mk3L coupled model simulations

The HC response to an increase in the anthropogenic greenhouse gas emissions found in several recent studies, using different datasets, is a weakening and a poleward expansion of this circulation (Lu et al. 2007, 2008, 2009; Hu and Fu 2007; Reichler and Held 2005; Seidel et al. 2008). Thus, we examine the impact of changes in both the strength and width of the HC upon stationary Rossby wave propagation using different scenarios of increasing CO_2 concentrations based on the coupled-model reference simulation.

A set of 3 experiments have been conducted. The first is the coupled-model reference run, which is integrated for 1000 years with the CO_2 concentration held constant at the preindustrial level (280 ppm). It is equivalent to the pre-industrial control used in CMIP5 experiments. The other two experiments, initialized from the coupled-model reference, are:

1. Idealized run with 1 % yearly increase of the CO_2 up to $4 \times CO_2$ levels (1120 ppm), hereafter denoted 1 %/year CO_2;
2. Three-member ensemble under instantaneous quadrupling of CO_2, hereafter denoted $4 \times CO_2$, from which we take the ensemble mean.

The reader is referred to Table 3 for a summary of the coupled simulations cited in this section. As for the

Table 2 Description of the atmosphere-model simulations used for the impacts analysis of changes in the HC width upon the stationary Rossby wave propagation

Simulations	Description
Atmosphere-model reference	Integrated for 140 years from 1871 to 2010 with time-evolving CO_2 concentration and observed SSTs (5-member ensemble)
TH30	Integrated for 140 years from 1871 to 2010 with time-evolving CO_2 concentration and observed SSTs with tropical heating (30°N–30°S) of 2 °C (5–member ensemble)
TH5	Integrated for 140 years from 1871-2010 with time-evolving CO_2 concentration and observed SSTs with tropical heating (5°N–5°S) of 2 °C (5–member ensemble)
ANOM30	Integrated for 140 years from 1871 to 2010 with time-evolving CO_2 concentration and observed SSTs with anomalies (30°N–30°S) (5-member ensemble)
ANOM5	Integrated for 140 years from 1871 to 2010 with time-evolving CO_2 concentration and observed SSTs with anomalies (5°N–5°S) (5-member ensemble)

Table 3 Description of the coupled-model simulations used for the impacts analysis of changes in the HC strength and width upon the stationary Rossby wave propagation

Simulations	Description
Coupled-model reference	Integrated for 1000 years with CO_2 concentration held constant at 280 ppm
1 %/year CO_2	Initialized from reference simulation, integrated for 140 years with 1 %/year yearly increase of the CO_2 concentrations up to 4 × CO_2 levels (1120 ppm)
4 × CO_2 − 1	Initialized from the end of year 200 of reference simulation, integrated until the year 700 with 4 × CO_2 concentrations (1120 ppm)
4 × CO_2 − 2	Initialized from the end of year 250 of reference simulation, integrated until the year 700 with 4 × CO_2 concentrations (1120 ppm)
4 × CO_2 − 3	Initialized from the end of year 300 of reference simulation, integrated until the year 700 with 4 × CO_2 concentrations (1120 ppm)

atmospheric simulations, the SH mean JJA climate fields for the difference between the perturbed ensemble mean and the coupled-model reference are analysed.

4 Assessing the skill of atmospheric simulations by the CSIRO Mk3L model

The JJA climatology for the reanalysis data and for the atmosphere-model reference ensemble over the period 1979–2010 is presented in order to verify how accurately the model simulates the observed HC, and the divergence and Rossby wave source fields. In the following sections the impacts of the simulated changes in the HC strength and width upon the stationary Rossby wave energy propagation are then discussed.

The distribution of the zonal mean meridional mass streamfunction (ψ) for JJA, computed from the reference ensemble and from the NCEP-DOE Reanalysis 2 dataset, is displayed in Fig. 2. The HC is the major component of the global mass circulation, which also consists of the Ferrel cell in mid-latitudes, and the polar cell in high latitudes. Figure 2a, based on the reanalysis dataset, shows a solstitial cell with counter-clockwise circulation in JJA, with ascent

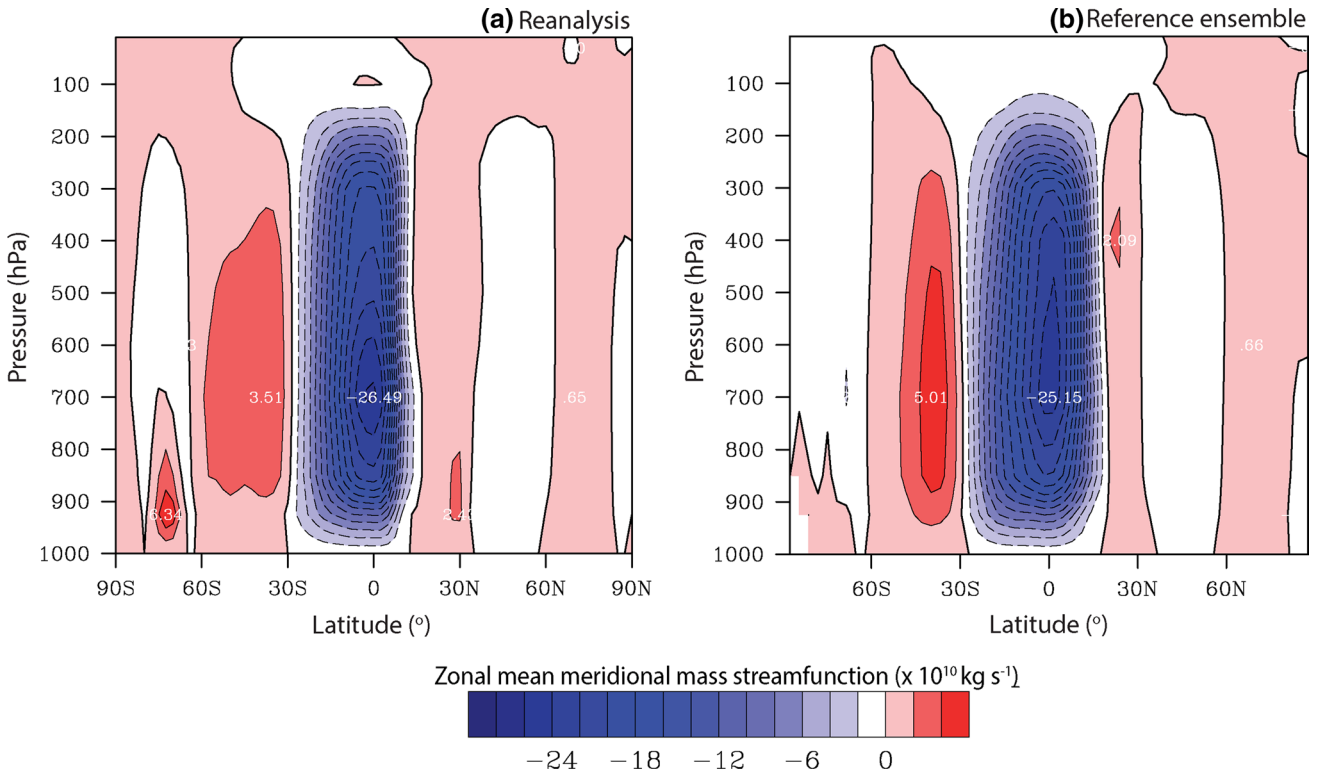

Fig. 2 Climatological average (1979–2010) for JJA of zonal mean meridional mass streamfunction (in units of 10^{10} kg s^{-1}) based on the (**a**) NCEP-DOE Reanalysis 2 dataset and (**b**) atmosphere-model reference ensemble mean. Contour intervals are 2 × 10^{10} kg s^{-1}. *Dashed* (*solid*) *lines* indicate negative (positive) values

near the Intertropical Convergence Zone (ITCZ) around 10°N (summer hemisphere) and subsidence around 30°S (winter hemisphere). We note that the reference ensemble, forced with observed SSTs and historical time-evolving CO_2 concentration, is able to give a realistic HC (Fig. 2b) compared to the reanalysis dataset (Fig. 2a).

The divergence field is a very useful diagnostic for quantifying changes in the strength of the HC. A weaker (stronger) HC leads to a smaller (larger) lifting mass and so, less (more) divergence in the upper troposphere. Longitudinal variability in the location and intensity of regions of divergence (positive values) and convergence (negative values) is depicted in Fig. 3a, b. The climatological field, based on the reanalysis dataset (Fig. 3a), shows a divergence area from 5° to 10°N over the Indian, Pacific and Atlantic Oceans, associated with the ITCZ, located further north in JJA. The divergence area is wider, extending from 10°S to 15°N, over the equatorial central-eastern Indian Ocean and Western Pacific. Intense divergence in JJA is found over Eastern Equatorial Pacific, near Central America, and around southern India, Thailand and Philippines (Fig. 3a). These climatological aspects were also noted by Freitas and Ambrizzi (2012).

The divergence field in the reference ensemble (Fig. 3b) is weaker compared to the reanalysis and the divergence zone from 5° to 10°N disappears in the central Pacific and Atlantic Oceans. The convergence over the South Indian Ocean is found to be located slightly further west compared with the observations (Fig. 3a).

The RWS climatological field in the austral winter (Fig. 3c, d) shows the largest values in the subtropics, around 25°S, over the western Pacific and over southern Australia to the south. Cyclonic (anticyclonic) vorticity is negative (positive) in the SH. Therefore, a negative (positive) value in the RWS field corresponds to a cyclonic (anticyclonic) source of Rossby waves. These results are consistent with studies of RWS using alternate reanalyses products by Shimizu and Cavalcanti (2011), Freitas and Ambrizzi (2012) and O'Kane et al. (2015). The negative values of the RWS field are found mainly over the subtropical east Pacific, Atlantic and Indian Oceans (Fig. 3c, d), with close similarity found between the reference ensemble and observations. The VS and AV components of the RWS are displayed in Fig. 4. The VS component is especially important in the extra-tropical regions (Fig. 4a, b), whereas the AV has major influence on the sources in the subtropical areas (Fig. 4c, d) and in particular regions of high barotropic–baroclinic instability over and to the west of the Tasman Sea (Frederiksen and Frederiksen 1993).

In summary, we note that the reference ensemble, forced with observed SSTs and historical time-evolving CO_2 concentration, is able to simulate a realistic HC and to skillfully reproduce the broad features of the fields of divergence, RWS and its components, compared with the reanalysis dataset.

5 Hadley circulation changes and impacts on stationary Rossby wave in atmosphere CSIRO Mk3L model

5.1 Changes in the HC strength

Table 4 shows the HC mean intensity for the WG and SG atmospheric simulations in the period 1979–2010 and for the difference (perturbed-reference). A strong (weak) SST gradient leads to an intensified (weakened) HC. This can be seen in Fig. 5, which shows the HC distribution computed from the difference between the perturbed and the reference ensemble means. The strengthening (weakening) of the HC is mainly observed near the equator in the SG (WG) simulation as it is linked to the changes in the divergence field.

Figure 6a shows that the divergence increases in the SG simulation, especially near Central America and over southern India, Thailand and Philippines. In the subtropics, a region of intense convergence anomaly around 90°E (see divergent wind vectors) and some regions of divergence anomaly around 30°E, 140°E and 20°W can be seen. Here, the word "anomaly" represents the difference between the perturbed and the reference ensemble means.

The main differences in the RWS field are near 30°S (Fig. 6b). The contribution to RWS in the equatorial region is small (Fig. 3c, d), as large divergence values found there (Fig. 3a, b) are counterbalanced by smaller values of the absolute vorticity (Shimizu and Cavalcanti 2011; Freitas and Ambrizzi 2012). Tyrrell and Karoly (1996) found that, although the upper level tropical divergence does not directly contribute to large RWS in the tropics, extra-tropical convergence regions, connected to the tropical convection, appear to be very important in the generation of Rossby waves at upper levels. Figure 6b indicates that the changes in the RWS field are linked to the changes in the divergence pattern. A cyclonic anomaly source is observed around 90°E (where earlier a convergence anomaly was found—Fig. 6a), and three anticyclonic anomaly sources are seen around 30°E, 140°E and 20°W (divergence anomaly zone). Hence, cyclonic (anticyclonic) anomaly sources are linked to the convergence (divergence) anomaly regions. These cyclonic and anticyclonic anomaly sources are primarily influenced by the VS component (Fig. 6c), whereas the AV role is comparatively small (Fig. 6d).

Figure 7 (a) shows that the divergence decreases in the WG simulation, with a change pattern almost opposite to that observed in the SG simulation over the regions of intense divergence near Central America and over southern

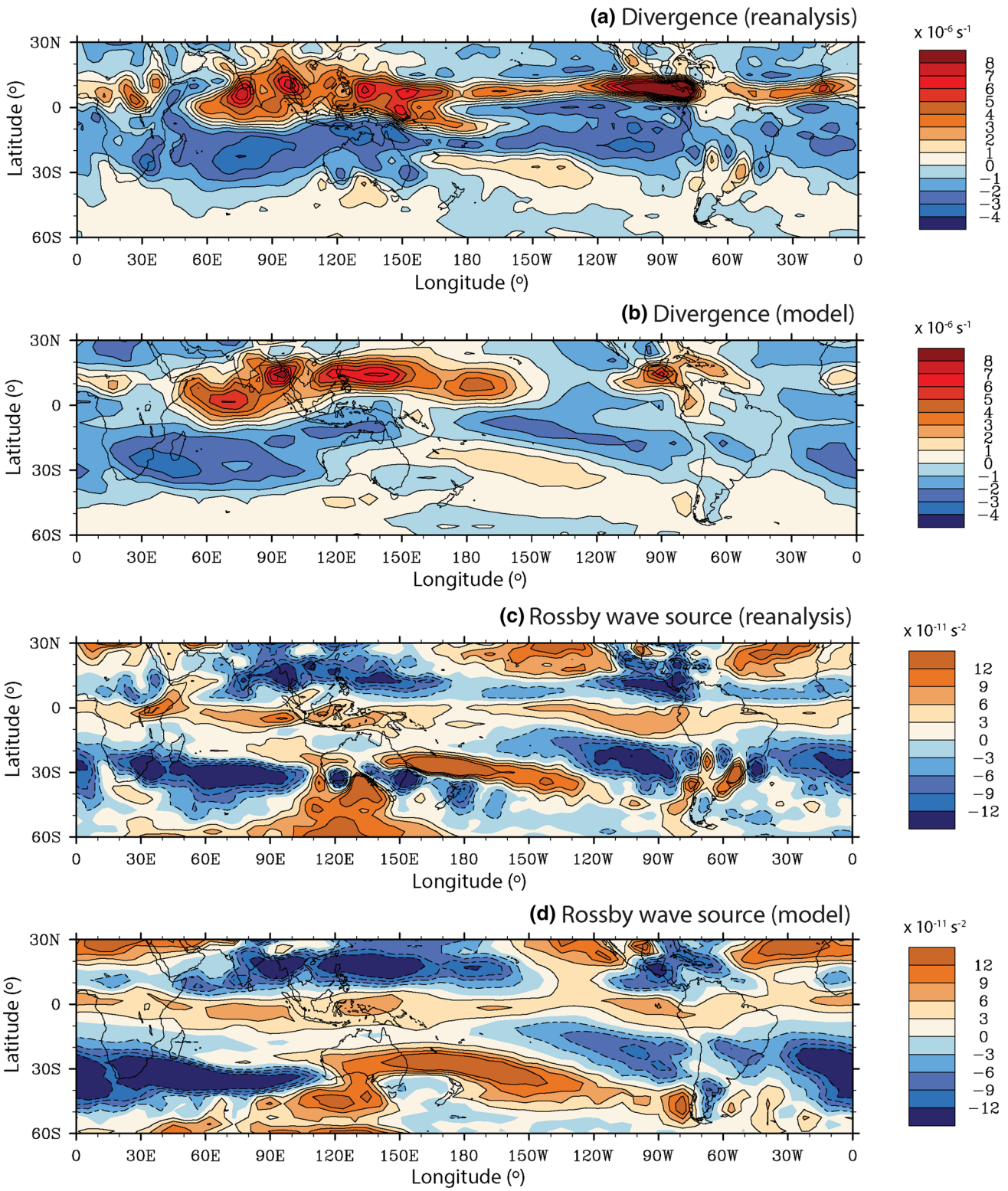

Fig. 3 Climatological average (1979–2010) for JJA of divergence (in units of 10^{-6} s^{-1}) at 200 hPa based on the: (**a**) NCEP-DOE Reanalysis 2 dataset, (**b**) atmosphere-model reference ensemble mean, and Rossby wave source (in units of 10^{-11} s^{-2}) based on the: (**c**) NCEP-DOE Reanalysis 2 dataset, (**d**) atmosphere-model reference ensemble mean. The divergence (Rossby wave source) plots have contour intervals of 1×10^{-6} s^{-1} (3×10^{-11} s^{-2})

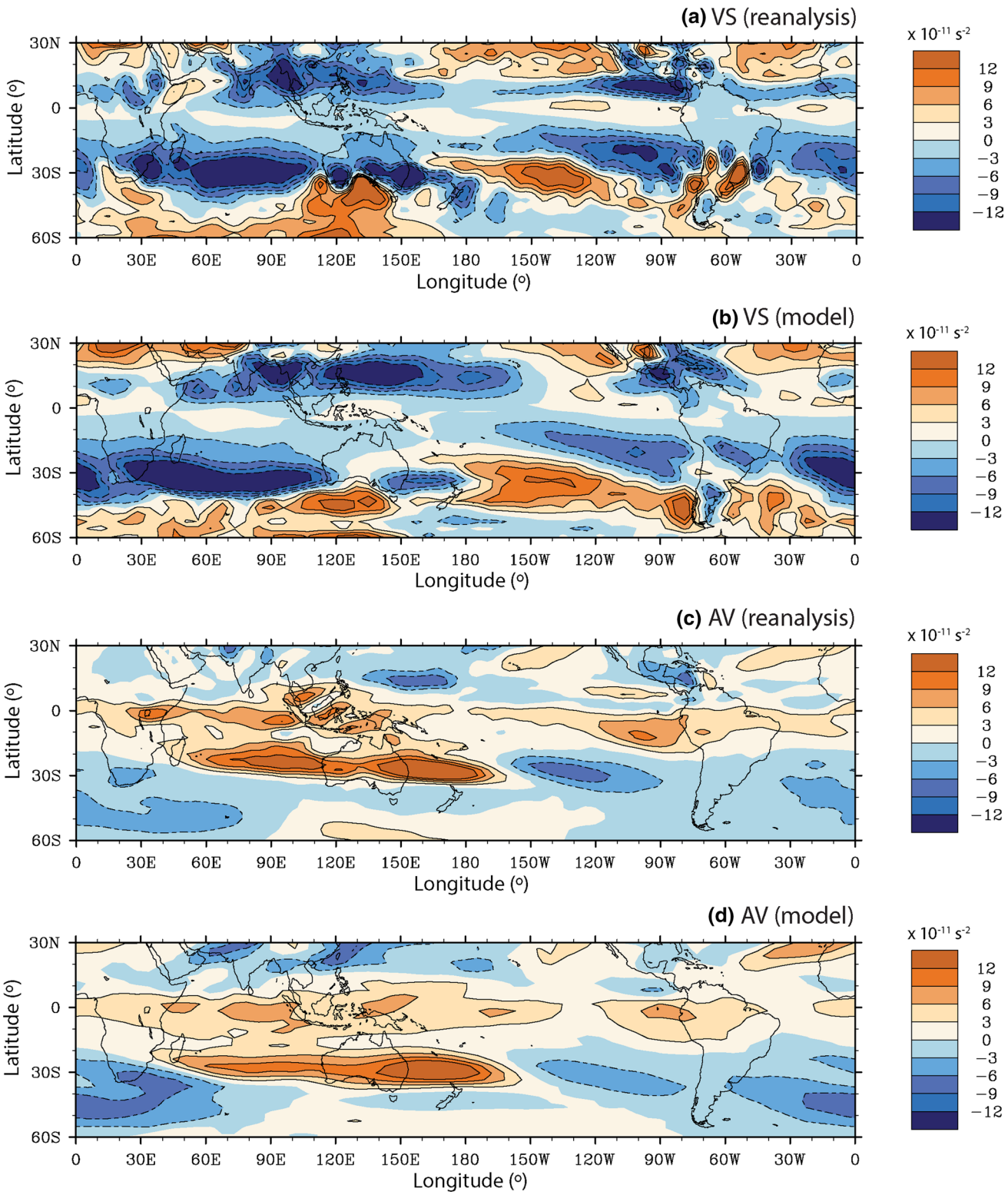

Fig. 4 Climatological average (1979–2010) for JJA of vortex stretching component (VS) at 200 hPa based on the: (**a**) NCEP-DOE Reanalysis 2 dataset, (**b**) atmosphere-model reference ensemble mean, and advection of absolute vorticity by divergent flow component (AV) based on the: (**c**) NCEP-DOE Reanalysis 2 dataset, (**d**) atmosphere-model reference ensemble mean. Contour intervals are 3×10^{-11} s^{-2}

Table 4 HC mean intensity (in units of 10^9 kg s^{-1}) and the difference (perturbed-reference) for the atmosphere-model simulations specified

Simulations	Mean intensity	Mean intensity difference (95 % confidence interval)
WG	−22.33	**2.96** (2.38 to 3.54)
SG	−35.08	**−9.79** (−10.30 to −9.27)

Values in bold are statistically significant at 5 % probability level according to Student's *t* test

+ (−) difference signal indicates weakening (strengthening) of the HC

India, Thailand and Philippines (c.f. Fig. 6a). In the subtropics, regions of intense divergence around 90°E and convergence around 140°E are seen (opposite to what was found for the SG simulation). Figure 7b indicates that these divergence changes in the WG simulation are also linked to the modifications in the RWS field. An anticyclonic anomaly source is seen around 90°E (divergence anomaly region), and a cyclonic anomaly source is observed around 140°E (convergence anomaly area). The VS component has an important role over these cyclonic and anticyclonic anomaly sources (Fig. 7c), with slight positive and negative contributions of the AV component primarily localised to the Tasman Sea and East Coast of Australia (Fig. 7d); as also verified for the SG simulation.

Figure 8 shows the stationary wave streamfunction field (with the zonal average removed) at 200 hPa for the difference between the perturbed ensemble mean (SG and WG simulations) and the reference ensemble. Negative (positive) values of this field represent ridges (troughs) in the SH. Due to the cyclonic (anticyclonic) anomaly sources (Figs. 6, 7), troughs (ridges) are found directly downstream from the convergence (divergence) anomaly regions in the subtropics. The stationary wave pattern is almost opposite between SG and WG simulations in the regions around South Africa and Madagascar, Australia, and south of South America; presenting some similarity with the observed results reported by Freitas and Ambrizzi (2012) using the NCEP/NCAR reanalysis dataset.

5.2 Changes in the HC width

Next, we specifically investigate the changes in the HC poleward extension, which is the precise latitude (obtained by linear interpolation) at which the average streamfunction

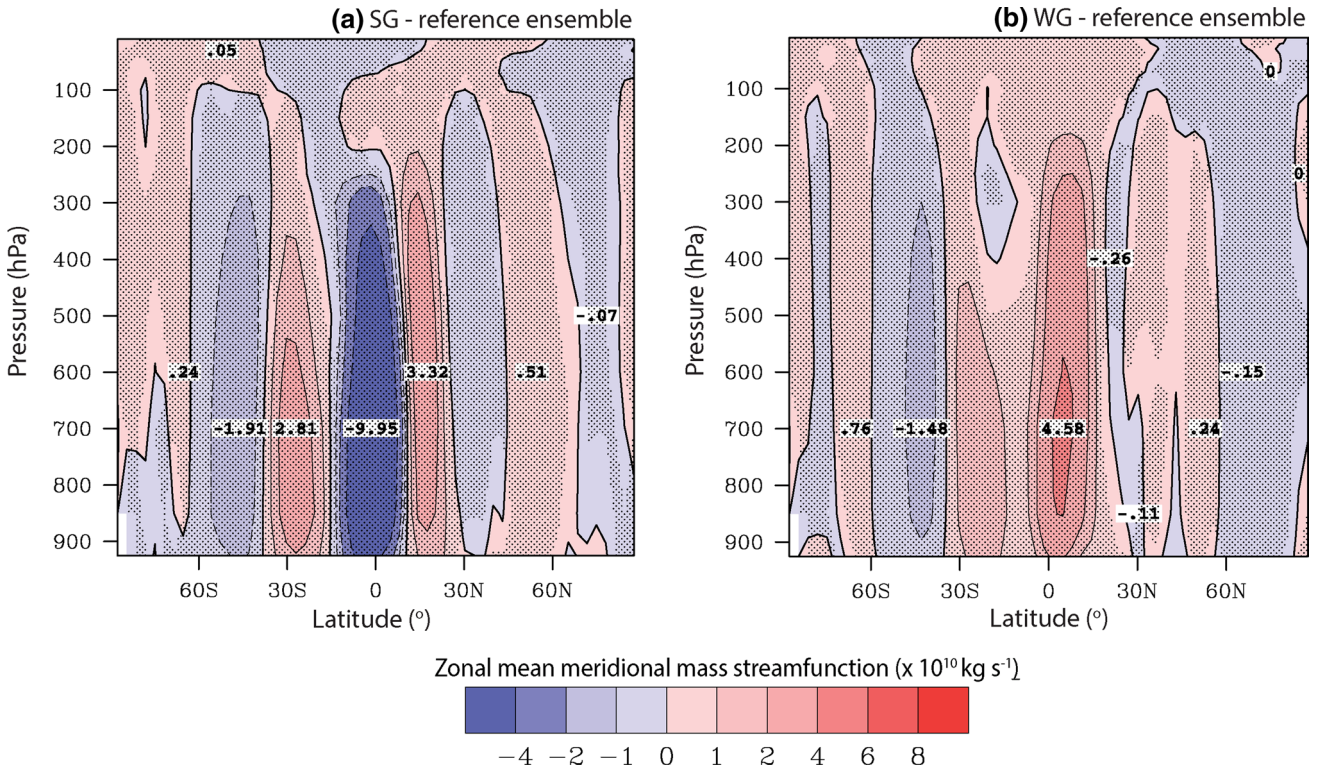

Fig. 5 Difference in JJA zonal mean meridional mass streamfunction (in units of 10^{10} kg s^{-1}) between the (**a**) SG and atmosphere-model reference ensemble means, (**b**) WG and atmosphere-model reference ensemble means. Contour intervals are 2×10^{10} kg s^{-1} with stippling indicating regions where the differences are statistically significant at the 5 % probability level as determined by Student's *t* test. *Dashed* (*solid*) *lines* indicate negative (positive) values

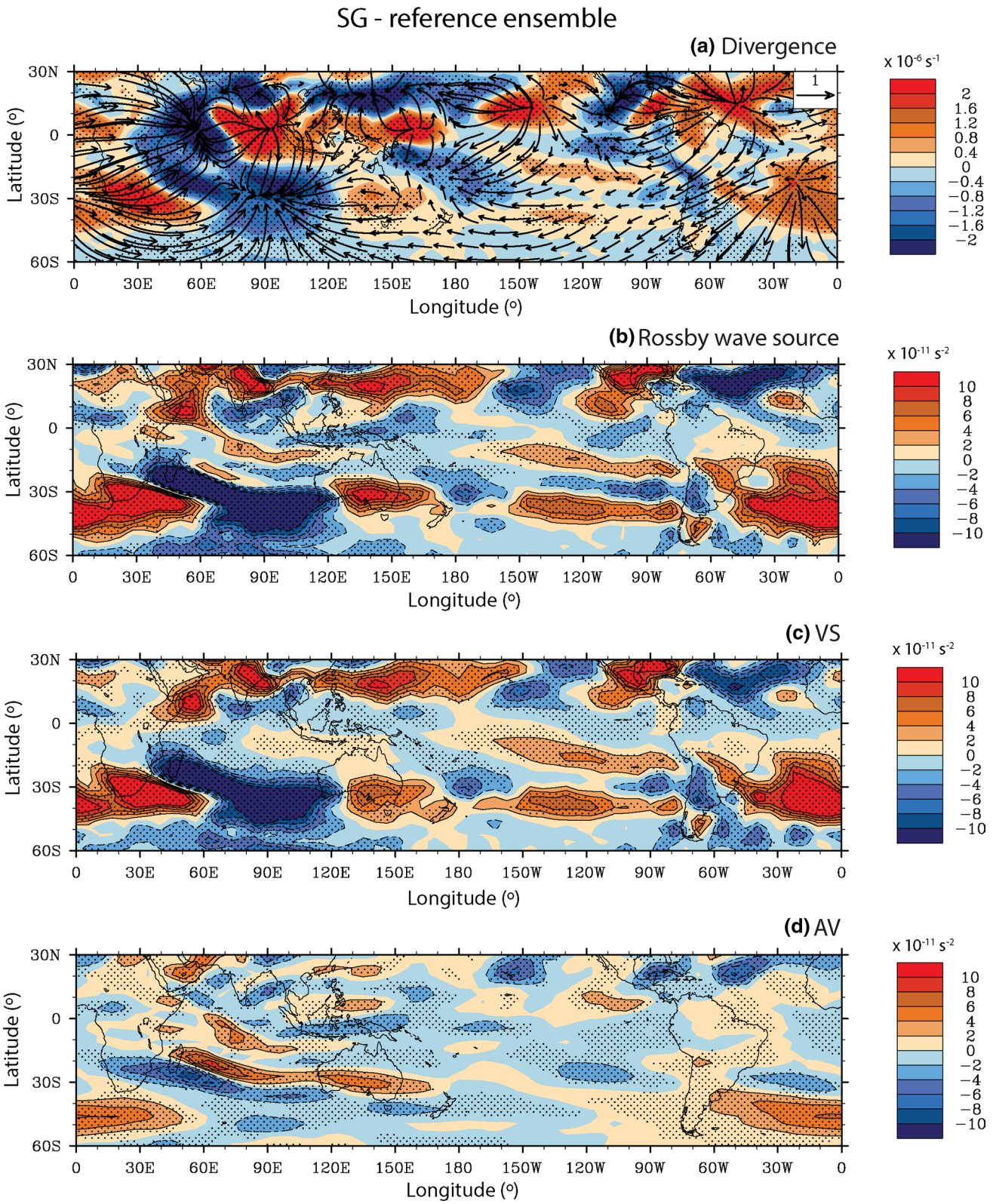

Fig. 6 Difference in JJA at 200 hPa between the SG and the atmosphere-model reference ensemble means for (**a**) divergence (in units of 10^{-6} s^{-1}) with the divergent wind vectors, (**b**) Rossby wave source (in units of 10^{-11} s^{-2}), (**c**) vortex stretching component (in units of 10^{-11} s^{-2}), (**d**) advection of absolute vorticity by divergent flow component (in units of 10^{-11} s^{-2}). Contour intervals are 0.4×10^{-6} s^{-1} and 2×10^{-11} s^{-2}, respectively, with stippling indicating regions where the differences are statistically significant at the 5 % probability level as determined by Student's *t* test

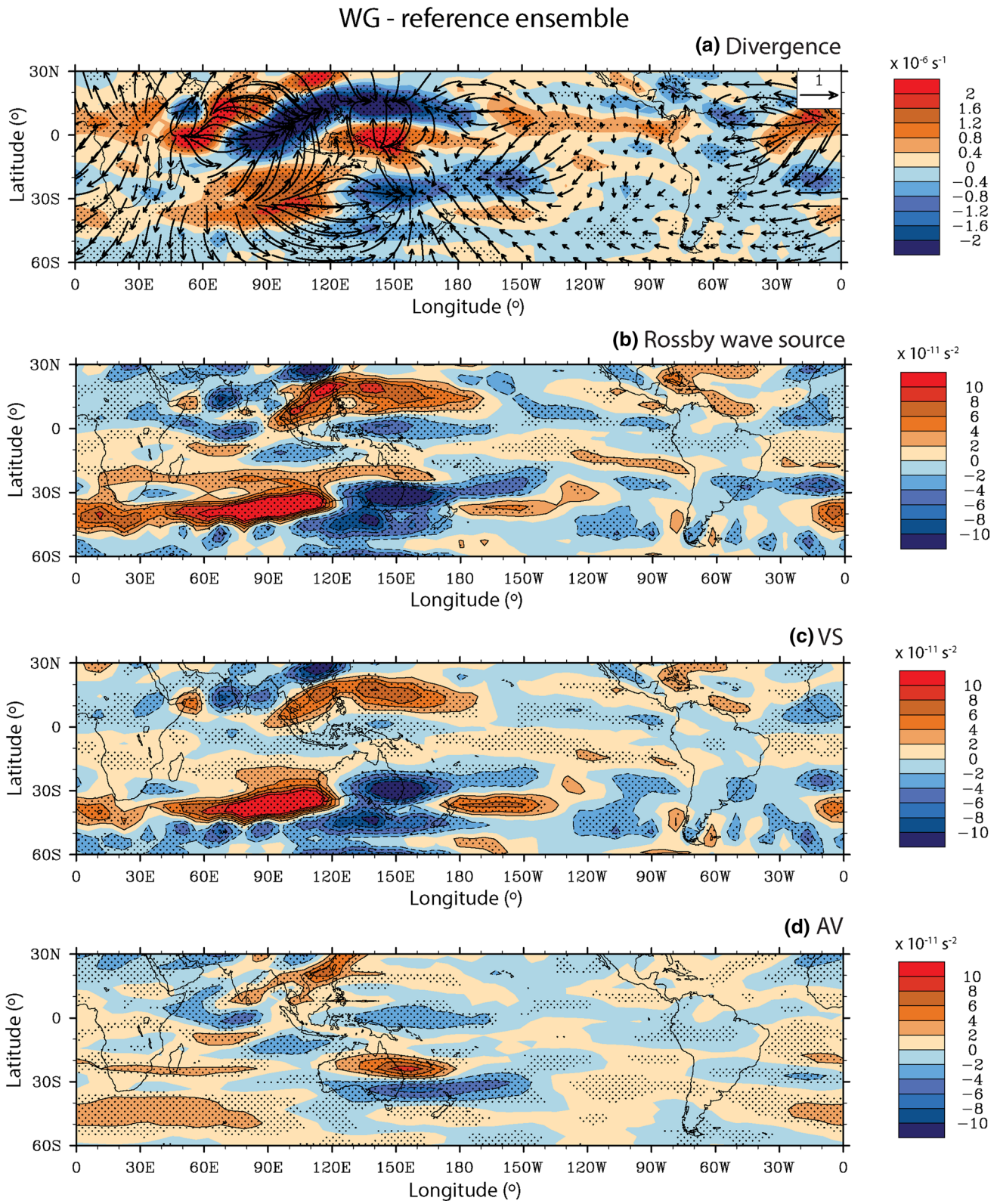

Fig. 7 As for Fig. 6 but for difference between the WG and the atmosphere-model reference ensemble means

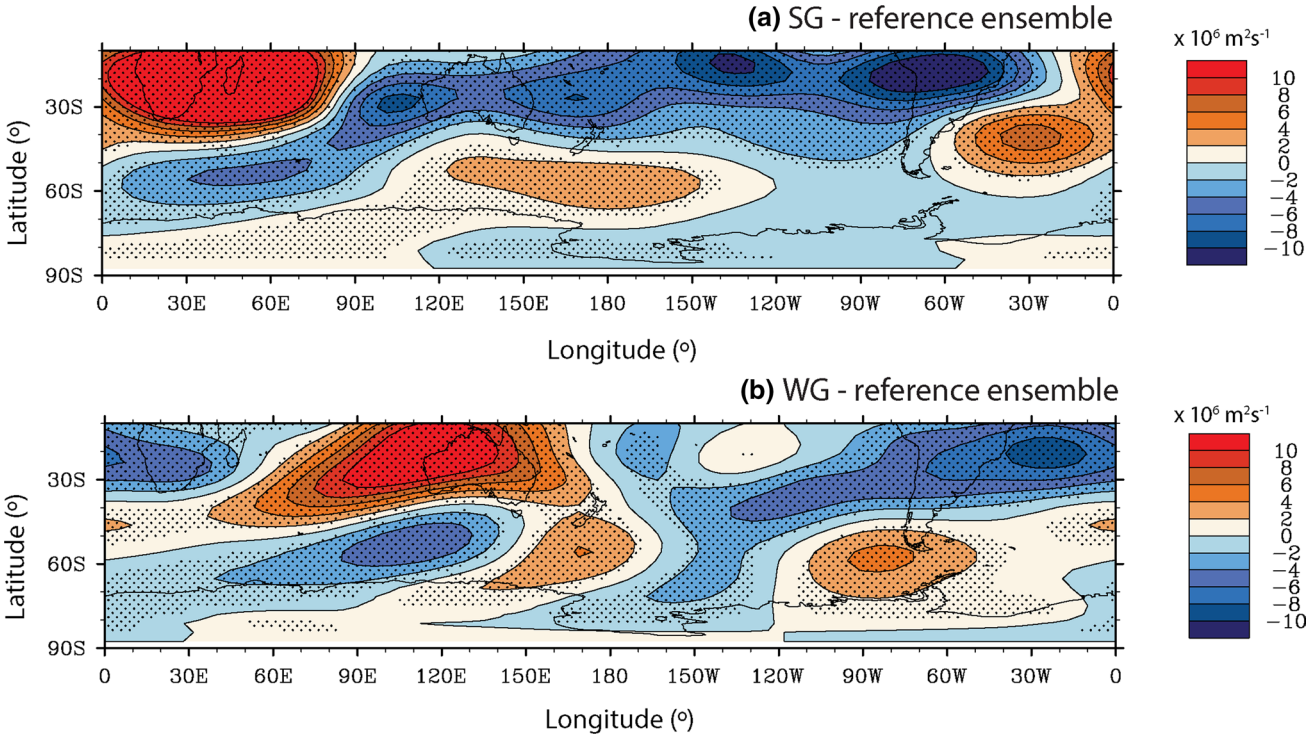

Fig. 8 Difference in JJA stationary wave streamfunction (in units of 10^6 m^2 s^{-1}) at 200 hPa between the (**a**) SG and atmosphere-model reference ensemble means, (**b**) WG and atmosphere-model reference ensemble means. Contour intervals are 2 × 10^6 m^2 s^{-1} with stippling indicating regions where the differences are statistically significant at the 5 % probability level as determined by Student's *t* test

Table 5 HC poleward extension (°latitude) and the difference (perturbed-reference) for the atmosphere-model simulations specified

Simulations	Poleward extent	Poleward extent difference (95 % confidence interval)
TH30	−31.08	**−1.21** (−1.33 to −1.09)
TH5	−27.06	**+2.80** (2.64 to 2.96)
ANOM30	−30.07	**−0.21** (−0.37 to −0.04)
ANOM5	−29.61	**+0.26** (0.09 to 0.43)

Values in bold are statistically significant at 5 % probability level according to Student's *t* test

+ (−) signal indicates °S (°N)

takes the value 0.0 at the pressure level of 500 hPa. The latitude of the extratropical boundary of the SH HC during JJA is used to diagnose the poleward position of the austral winter HC. Table 5 shows the climatological HC poleward extension for the TH30, TH5, ANOM30 and ANOM5 simulations and for the difference (perturbed-reference). Tandon et al. (2013), using an idealized GCM, verified that a thermal forcing applied to a narrow region around the equator produced HC contraction and equatorward shift of the jets, while a forcing with wider meridional extent produced HC expansion and poleward shift of the jets. Thus, Table 5 shows, through the difference in the poleward extent, that the TH30 simulation, which was constructed considering a wide SST warming (30°S–30°N), produces a poleward shift of the extratropical boundary of the SH HC. On the other hand, the TH5 simulation, with a narrow SST warming, produces an equatorward shift. The same results can be verified for the ANOM30 and ANOM5 simulations. The dipole structure around 30°S in Figs. 9a and 10a also reveals the poleward shift of the extratropical boundary of the SH HC. We note that the results for the TH30 (TH5) simulation are similar to the ANOM30 (ANOM5) simulation, but the magnitude of the differences between the perturbed and the reference ensemble mean is much larger in the former case.

Figures 9a and 10a show clearly an upward shift of the HC, not so evident in Figs. 9b and 10b since the SST warming is narrow (5°S–5°N) in these cases. The upper boundary of the HC corresponds to the tropopause of the atmosphere. Both the tropopause and the upper boundary of the HC rise in a warmer climate (Gastineau et al. 2008). A weakening of the HC is also seen for all simulations considered here (TH30, TH5, ANOM30, ANOM5). This is because the warmer climate by itself actually leads to a decrease in HC intensity, as found by Rind and Perlwitz (2005). We will discuss this issue in greater detail in Sect. 6.

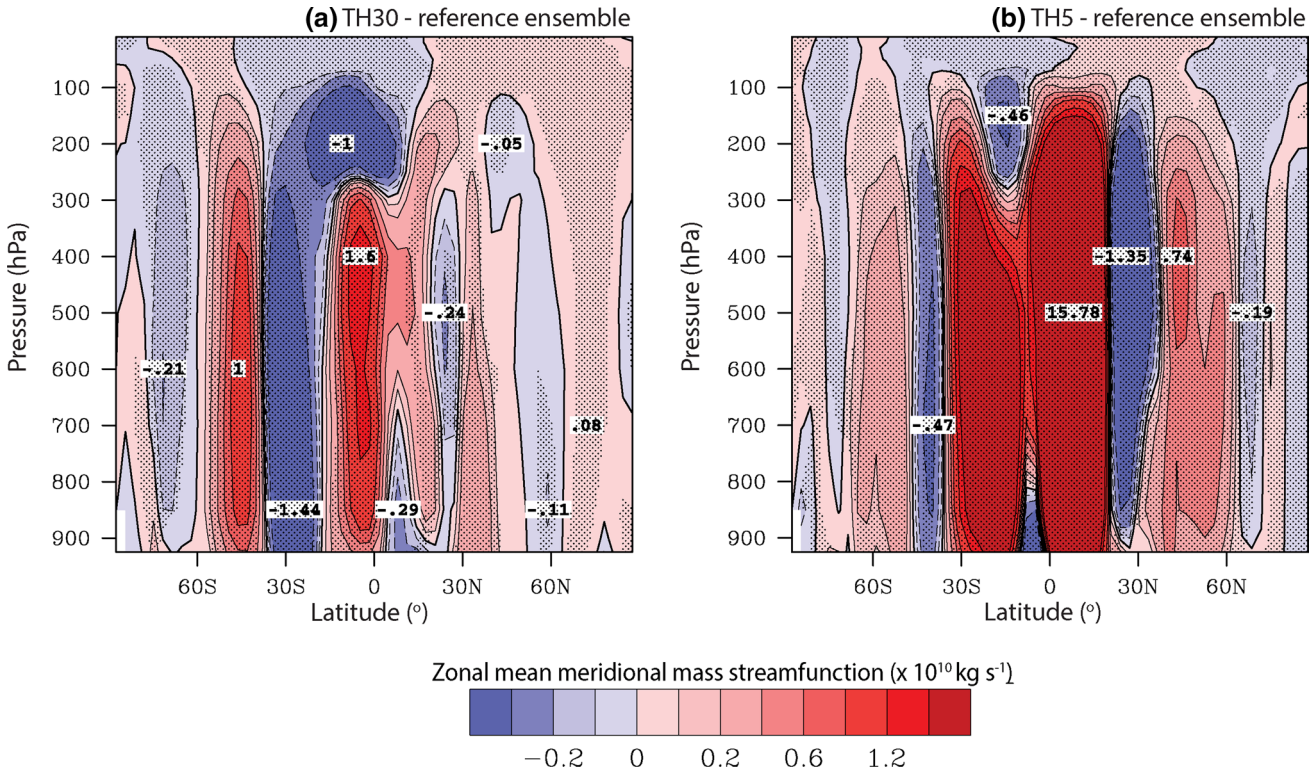

Fig. 9 Difference in JJA zonal mean meridional mass streamfunction (in units of 10^{10} kg s^{-1}) between the (**a**) TH30 and atmosphere-model reference ensemble means, (**b**) TH5 and atmosphere-model reference ensemble means. Stippling indicating regions where the differences are statistically significant at the 5 % probability level as determined by Student's *t* test. *Dashed* (*solid*) *lines* indicate negative (positive) values

The divergence field for the TH30 simulation (Fig. 11a) is weaker than for the TH5 simulation (Fig. 11b). The same is observed for the ANOM30 and ANOM5 simulations (Fig. 11c, d). As well, the divergence field in the TH30 (TH5) simulation is more intense in relation to the ANOM30 (ANOM5) simulation (Fig. 11). The differences between the ANOM30 and ANOM5 simulations are small (Fig. 11c, d). In fact, we verified earlier (Table 5) that the poleward (equatorward) shift of the extratropical boundary of the SH HC is small in both these simulations.

The TH30 simulation shows a zonal dipole around 5°N, with a convergence anomaly zone from 10° to 90°E and a divergence anomaly sector from 90° to 140°E (Fig. 11a), whereas the TH5 simulation shows a convergence anomaly zone from 50°E to 140°W at 5°N and a divergence anomaly sector around the equator from 70°E to 150°W (Fig. 11b). This is the only substantive contrast seen in the divergence field between the ANOM30 and ANOM5 simulations (Fig. 11c, d). These simulations also show convergence anomaly regions from 50°E at 45°S towards the northeast of Australia around 20°S, and from 180° to 120°W around 40°S (Fig. 11c, d). Divergence anomaly sectors are seen in both simulations (ANOM30 and ANOM5) over the Atlantic Ocean and South Africa around 30°S, southeast Australia to the south, and over the West Pacific Ocean from 30° to 60°S (Fig. 11c, d). These convergence and divergence anomaly zones are also seen in the TH30 simulation (Fig. 11a).

As noted earlier, the divergence changes are linked to the modifications in the RWS field. Again, anticyclonic (cyclonic) anomaly sources are seen over the regions of divergence (convergence) anomaly (Fig. 12). These cyclonic and anticyclonic anomaly sources are mostly associated with the VS component, but there are positive contributions of the AV component to the RWS total field mainly over the Atlantic Ocean, South Africa, southeast of Australia, and from 45°S, 50°E stretching towards eastern Australia at around 30°S in the TH30 and ANOM30 simulations (not shown). Positive influences of the AV component in the TH5 and ANOM5 simulations are seen mainly over the southern tip of Africa around 30°S, and from south of Madagascar towards southeast Australia to 150°W (not shown) associated with the subtropical jet, which acts as a Rossby waveguide (Hoskins and Ambrizzi 1993).

The stationary wave streamfunction fields for the TH30 and TH5 simulations are displayed in Fig. 13a, b. The wave pattern at mid-high latitudes for the TH30 simulation is very similar to what was found by Marshall and Connolley

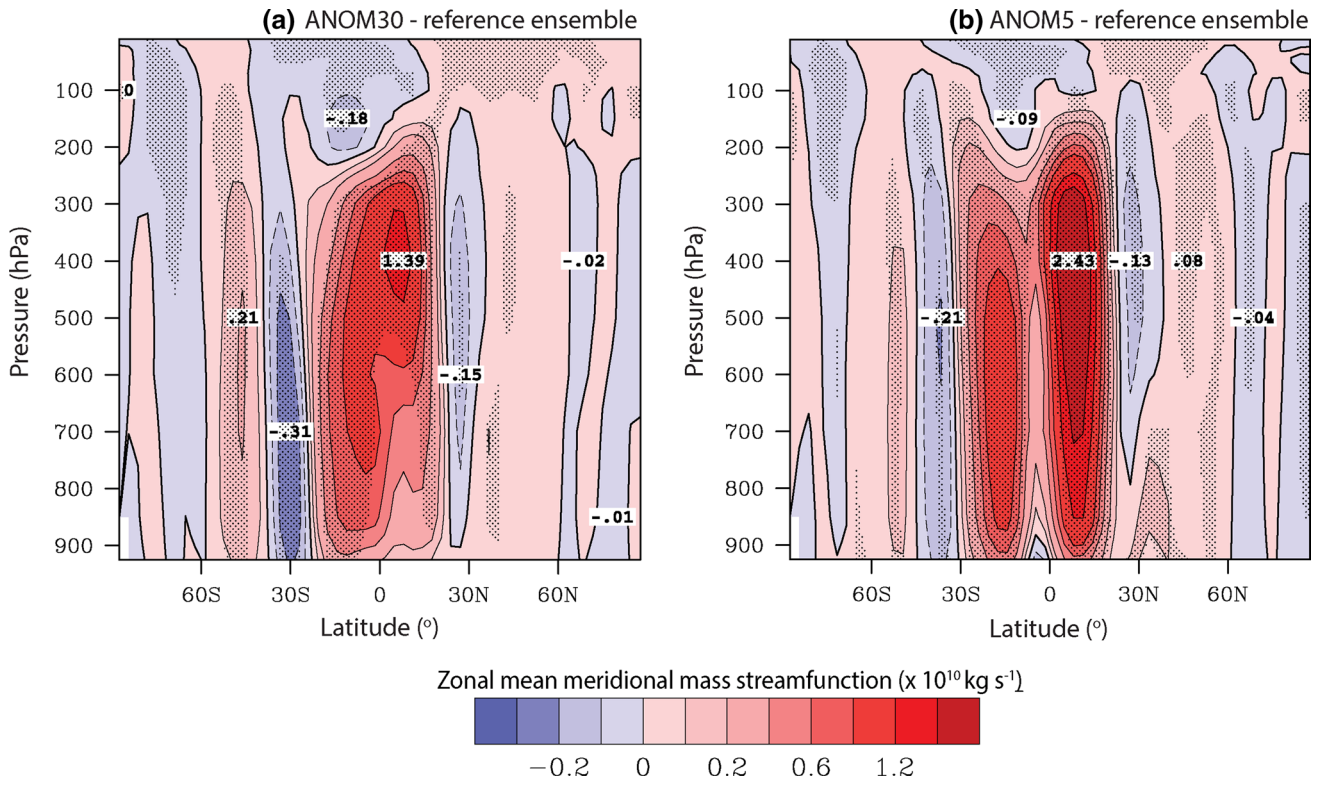

Fig. 10 As Fig. 9 but for difference between the (**a**) ANOM30 and atmosphere-model reference ensemble means, (**b**) ANOM5 and atmosphere-model reference ensemble means

(2006, Fig. 2a) in their idealized experiment, where the tropical ocean SSTs were increased. These authors examined the impact that changes in the winter SH SST gradient have on the sign and strength of the SH Annular Mode (SAM). According to them, changes in winter tropical SSTs have little direct influence on the SAM, but they do force a strong wave train across the Southern Ocean, which has similarities to the PSA pattern.

The TH5 simulation shows stronger and eastward shifted troughs and ridges (Fig. 13b) in relation to the TH30 simulation (Fig. 13a). This is because the cyclonic and anticyclonic anomaly sources in the TH5 simulation are stronger and very zonally extended (Fig. 12b) in relation to the TH30 simulation (Fig. 12a). The lack of significant differences, mainly in the divergence field, between the ANOM30 and ANOM5 simulations is reflected in the structure of the stationary wave streamfunction field at 200 hPa (Fig. 13c, d). However, the ANOM5 simulation exhibits stronger troughs and ridges (Fig. 13c in comparison with the ANOM30 simulation (Fig. 13d), largely due to stronger cyclonic and anticyclonic anomaly sources (Fig. 12c, d). On the other hand, these anomaly sources in the ANOM5 simulation are not as zonally extended as in the TH5 simulation. Therefore, it is very likely that the SST anomalies outside the latitude band of 5°S–5°N do not significantly affect the spatial pattern of the stationary Rossby wave propagation.

6 Hadley circulation changes and impacts on stationary Rossby waves in coupled CSIRO Mk3L model

O'Kane et al. (2013a, b) showed that the entire Southern Ocean thermocline, as well as the boundary currents, underwent a systematic regime transition around 1978 associated with a more dominant positive phase of the SAM and a reduction in the persistence of the positive phase of the hemispheric wavenumber three blocking pattern. Recently, it has been shown that, when all seasons are considered, CO_2 is the dominant external covariant driving the observed secular trends in wave 3, SAM and blocking (Franzke et al. 2015; O'Kane et al. 2015). As mentioned earlier in Sect. 3.3.2, the global and annual mean SST, according to the HADISST dataset, has broadly increased from 1870 to 2010, with a significant positive trend of 0.04 °C per decade. As well, Freitas et al. (2015) found, using non-stationary vector autoregressive clustering techniques, that the southern ocean (south of 30°S) underwent a major regime transition in the late 1970s, when

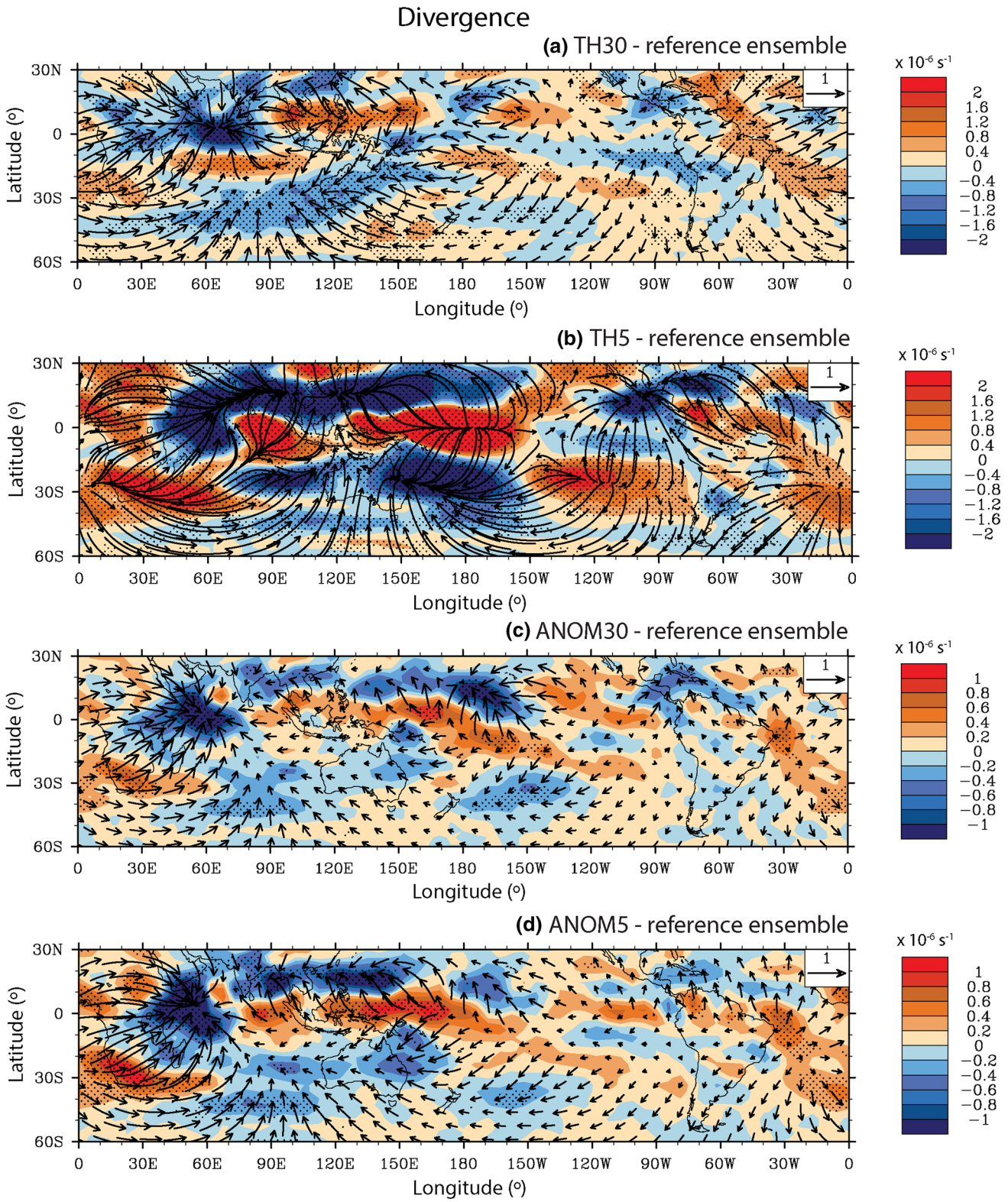

Fig. 11 Difference in JJA divergence (in units of 10^{-6} s^{-1}) with the divergent wind vectors at 200 hPa between the (**a**) TH30 and atmosphere-model reference ensemble means, (**b**) TH5 and atmosphere-model reference ensemble means, (**c**) ANOM30 and atmosphere-model reference ensemble means, (**d**) ANOM5 and atmosphere-model reference ensemble means. Contour interval is 0.4×10^{-6} s^{-1} for (**a**) and (**b**), 0.2×10^{-6} s^{-1} for (**c**) and (**d**), with stippling indicating regions where the differences are statistically significant at the 5 % probability level as determined by Student's *t* test

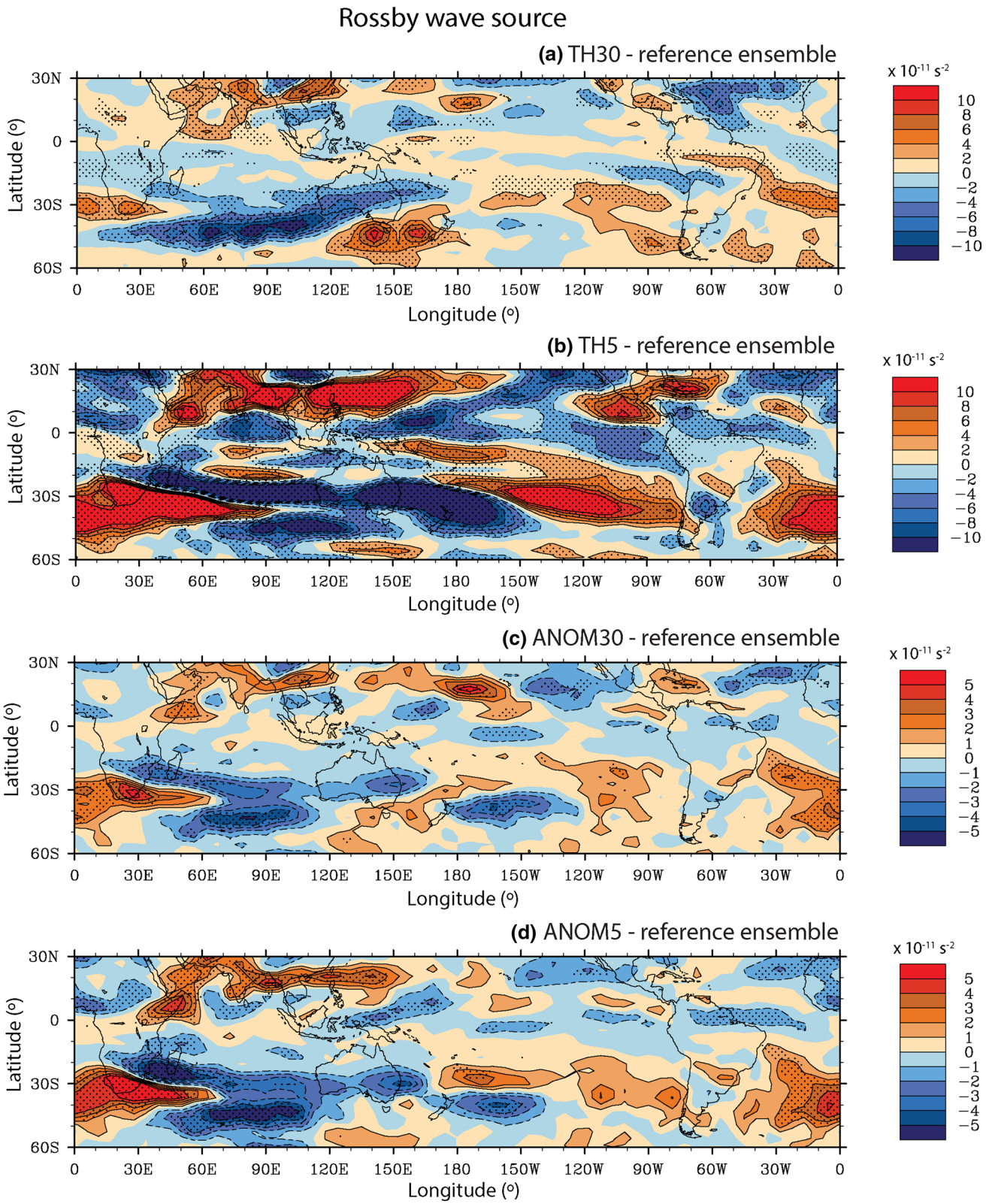

Fig. 12 As for Fig. 11 but for Rossby wave source (in units of 10^{-11} s^{-2}). Contour interval is 2×10^{-11} s^{-1} for (**a**) and (**b**), 1×10^{-11} s^{-1} for (**c**) and (**d**)

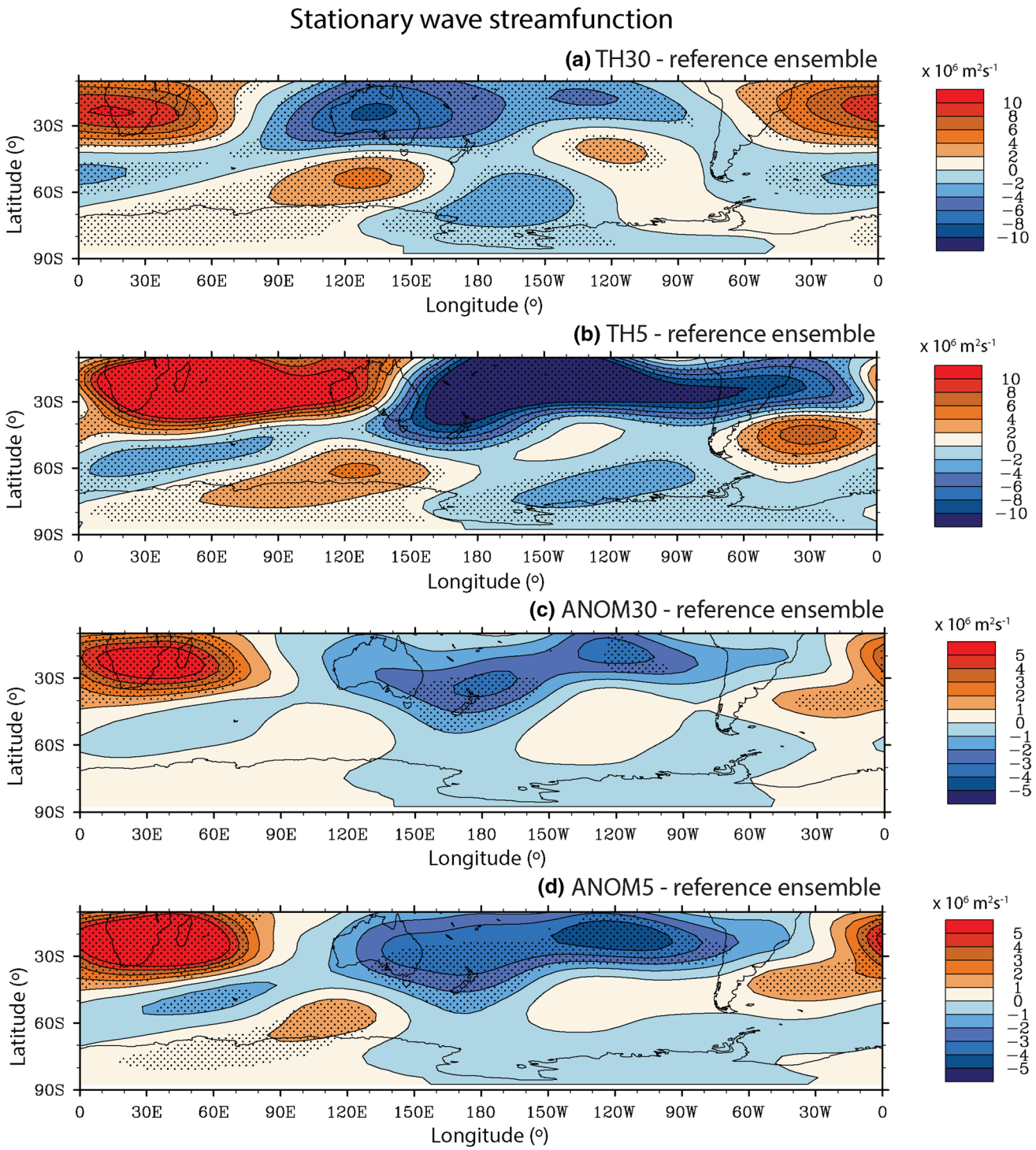

Fig. 13 As for Fig. 12 but for stationary wave streamfunction (in units of 10^6 m^2 s^{-1}). Contour interval is 2 × 10^6 m^2 s^{-1} for (**a**) and (**b**), 1 × 10^6 m^2 s^{-1} for (**c**) and (**d**)

the Indian Ocean and western boundary currents warmed and this is unlike the decadal variability of the preceding century. According to them, the transition between decadal variability and the preference for a warm SST state since the late 1970s suggests that the SST is carrying some of the signal of the CO_2 increase, and thus, it is reasonable to assume that the observed changes in the SST are not just due to the decadal variability, but have a contribution from increasing greenhouse gases. Therefore, there is an indirect effect of the anthropogenic CO_2 forcing (via changes

Table 6 HC mean intensity (in units of 10^9 kg s^{-1}) for the last 40 years of the coupled-model simulations considered with the difference (perturbed-reference) and its linear trend (in units of 10^9 kg s^{-1} per decade)

Simulations	Mean intensity	Mean intensity difference (95 % confidence interval)	Mean intensity difference linear trend (95 % confidence interval)
1 %/year CO_2	−23.70	**1.96** (1.37 to 2.55)	**+0.72** (0.23 to 1.21)
4 × CO_2	−23.28	**2.38** (1.93 to 2.82)	+0.33 (−0.05 to 0.72)

Values in bold are statistically significant at 5 % probability level according to Student's *t* test

+ trend signal indicates weakening of the HC

Table 7 HC poleward extension (°) for the last 40 years of the coupled-model simulations considered with the difference (perturbed-reference)

Simulations	Poleward extent	Poleward extent difference (95 % confidence interval)
1 %/year CO_2	−30.35	**−0.69** (−0.91 to −0.48)
4 × CO_2	−30.48	**−0.83** (−0.98 to −0.67)

Values in bold are statistically significant at 5 % probability level according to Student's *t* test

+ (−) signal indicates °S (°N)

in SST) that might be important in the case of atmospheric simulations.

Several studies have found that global warming produces both expansion and weakening of the HC (e.g. Lu et al. 2008, 2009; Gastineau et al. 2008). Thus, next we investigate the impact of simulated changes in both the strength and width of the HC upon stationary Rossby waves using coupled simulations. A significant advantage of the AOGCM is that it simulates, as in the real world, the influence of the ocean on the overlying atmosphere and its response to fluctuations in surface heat fluxes driven by atmospheric variability. It also contains both the direct effects of anthropogenic CO_2 forcing (via differential changes in atmospheric heating) and the indirect effects (via changes in SST) (Deser and Phillips 2009).

Table 6 presents the HC mean intensity for the last 40 years of the 1 %/year CO_2 and 4 × CO_2 coupled simulations and for the difference (perturbed-reference). The weakening of the HC for the JJA season, under a global warming scenario, is of the order 7.6 % for the 1 %/year CO_2 simulation and 9.3 % for the 4 × CO_2 simulation. The amplitude of the 4 × CO_2 response is larger, as could be expected from a stronger radiative forcing. However, the 1 %/year CO_2 simulation presents a significant weakening trend of 0.72 × 10^9 kg s^{-1} per decade, whereas the trend for the 4 × CO_2 simulation is smaller and not significant. According to some studies (Caldeira and Myhrvold 2013; Gabriel and Robock 2015), approximately half of the warming under a 4 × CO_2 scenario occurs within the first decade and then a relatively slow trend develops for the next 50 years during which another approximately one quarter of the total warming occurs. We verified that the warming in the 4 × CO_2 simulation is nearly 3 times greater in the first decade than in the 1 %/year CO_2 simulation. Thus, the different pace of warming in the two scenarios considered here could explain the differences in the weakening HC trends calculated for the last 40 years of the coupled-model simulations.

The results for the poleward extension in the coupled-model simulations are presented in Table 7. The poleward shift of the extratropical boundary of the austral winter HC is about 0.7 degrees for 1 %/year CO_2 and 0.8 degrees for 4 × CO_2, considering the last 40 years of the simulations. Figure 14 corroborates these results, demonstrating the weakening of HC (around the equator), the poleward shift of the extratropical boundary (dipole around 30°S), and also the upward shift of the HC, as also verified for the TH30 and ANOM30 simulations (Figs. 9a, 10a). The differences are much stronger in the 4 × CO_2 simulation, as this scenario represents a dramatic and abrupt change in the radiative forcing.

The fields of divergence, RWS and stationary wave streamfunction for the 1 %/year CO_2 simulation [Fig. 15] are spatially very similar to the 4 × CO_2 [Fig. 16], but weaker. Thus, under a global warming scenario, the divergence field is characterized by a dipole around 5°S over the Indian Ocean, with a decrease to the north and an increase to the south in both simulations (Figs. 15a, 16a). Important convergence anomaly zones are seen around 35°S over the Indian Ocean and over the West Pacific around 30°S, whereas divergence anomaly zones are seen over the Atlantic Ocean, South Africa and East Pacific around 30°S, and over southern Australia to the south (Figs. 15a, 16a). Here, as for the AGCM simulations, anticyclonic and cyclonic anomaly sources (Figs. 15b, 16b) are observed over the regions of divergence and convergence anomalies (Figs. 15a, 16a), respectively. The VS component has the major influence over these cyclonic and anticyclonic anomaly sources, but there are positive contributions of the AV component to the RWS total field mainly over the South Africa and at 50°S from 50°E towards eastern Australia around 30°S for both simulations (not shown), similar to the findings for the TH30 and ANOM30 AGCM simulations. Positive contributions are also seen over southern Australia to the south in the 1 %/year CO_2 simulation and over southeast Australia in 4 × CO_2 (not shown).

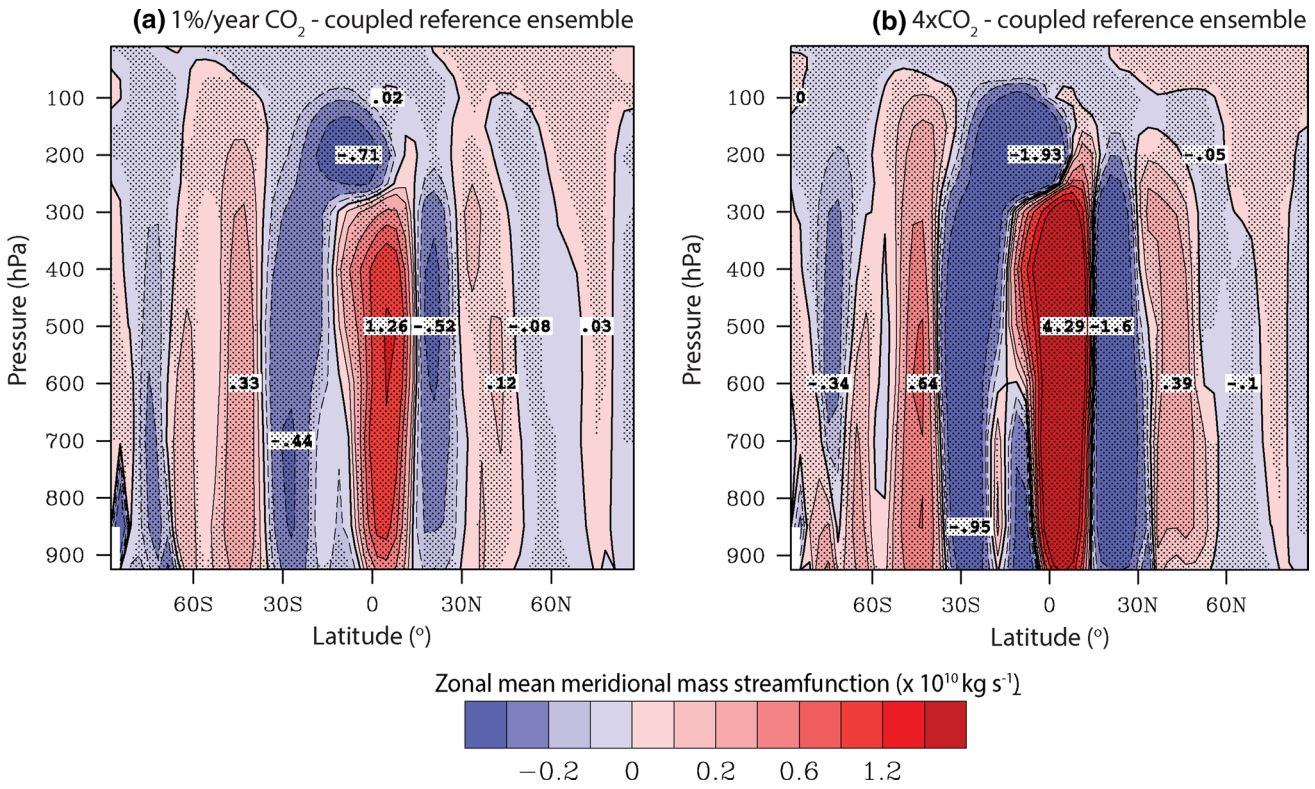

Fig. 14 Difference in JJA zonal mean meridional mass streamfunction (in units of 10^{10} kg s^{-1}) between the (**a**) 1 %/year CO_2 and coupled-model reference ensemble means, (**b**) 4 × CO_2 and coupled-model reference ensemble means. *Stippling* indicating regions where the differences are statistically significant at the 5 % probability level as determined by Student's *t* test. *Dashed* (*solid*) *lines* indicate negative (positive) values

The stationary wave streamfunction field for both simulations (Figs. 15c, 16c) shows a wave pattern at mid-high latitudes with troughs (ridges) directly downstream from the cyclonic (anticyclonic) sources. Important troughs are seen over South Africa, Atlantic Ocean and East Pacific around 30°S and to the south of Australia and central Pacific around 55°S (Figs. 15c, 16c). Ridges are seen over the Australian continent, Western Pacific, Eastern Indian Ocean around 30°S, south of South America, to the south of South Africa (Figs. 15c, 16c). The wave pattern is stronger in the 4 × CO_2 simulation (Fig. 16c) and is very similar to what was found in the TH30 atmospheric simulation (Fig. 13a). The fact that some similarity exists between the coupled and atmosphere-only simulations, in the case of wider SST warming (TH30 simulation), which represent a warmer climate, indicates a high degree of consistency between these simulations.

7 Discussion and conclusions

In this paper we have examined how simulated changes in the strength and width of the austral winter HC, induced by anomalous SST gradients and changes in CO_2 concentrations, affect the extra-tropical atmospheric circulation, and in particular, stationary Rossby wave propagation. The effect of the changes in the HC upon stationary Rossby wave propagation is indirect, i.e., via the deep convection in the rising branch of the HC and the associated anomalous divergence at high levels. We have analysed this indirect effect through directly applying changes in the tropical SST pattern and radiative forcing. The RWS and upper level mid-latitude circulation responses associated with the tropical convection have been investigated here using a methodology similar to that of Tyrrell and Karoly (1996). As in Freitas and Ambrizzi (2012), it has been shown here that directly downstream from the convergence (divergence) anomaly regions in the subtropics, there are troughs (ridges) due to the cyclonic (anticyclonic) anomaly sources. Our results also show that atmospheric only simulations with observed SSTs are able to produce a quite realistic HC while reproducing the broad features of the climatological fields of divergence, RWS and its contributing components as compared with the NCEP-DOE Reanalysis 2 dataset.

In order to elucidate the various mechanisms and interactions responsible for controlling the strength and width

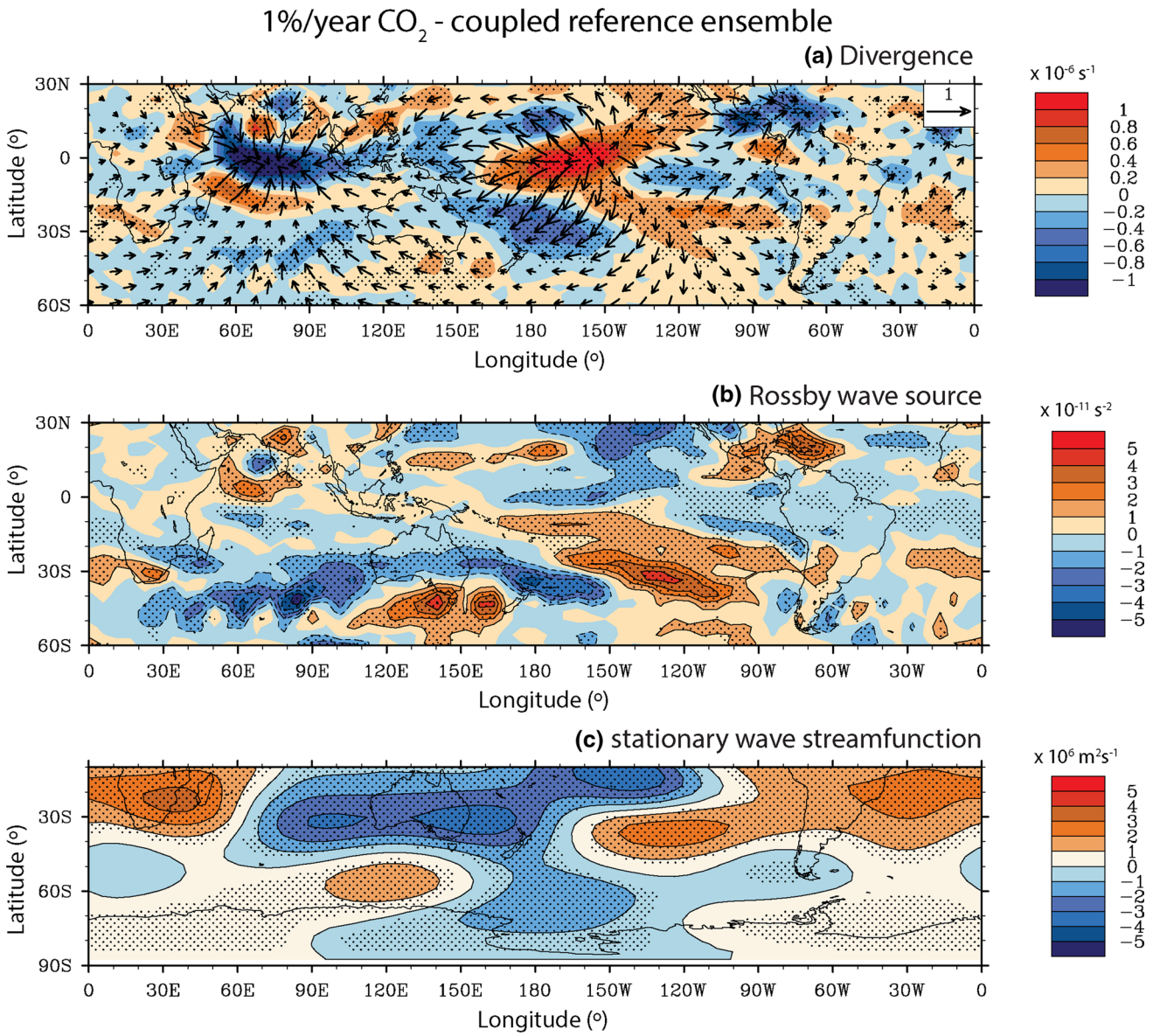

Fig. 15 Difference in JJA at 200 hPa between the 1 %/year CO_2 and coupled-model reference ensemble means for (**a**) divergence (in units of 10^{-6} s^{-1}) with the divergent wind vectors, (**b**) Rossby wave source (in units of 10^{-11} s^{-2}), (**c**) stationary wave streamfunction (in units of 10^6 m^2 s^{-1}). Contour intervals are 0.2×10^{-6} s^{-1}, 1×10^{-11} s^{-2} and 1×10^6 m^2 s^{-1}, respectively, with stippling indicating regions where the differences are statistically significant at the 5 % probability level as determined by Student's *t* test

of the HC we have first analysed separately and comprehensively the response of stationary Rossby wave propagation using an ensemble of idealized SST perturbations in an AGCM. A set of idealized SST perturbations were applied in order to induce responses in the strength and width of the HC. Specifically, both strong and weak SST gradients (SG and WG, respectively) were applied to investigate the response of the HC intensity. The simulated stationary Rossby wave propagation in both the SG and WG cases were consistent with some observed results reported earlier by Freitas and Ambrizzi (2012) using the NCEP/NCAR reanalysis. Both the narrower and wider SST warming (TH5 and TH30, respectively) were applied to induce responses in the HC width (poleward extension). A narrower SST warming produces stronger and very zonally extended response in the RWS, leading to stronger and eastward shifted troughs and ridges. A SST forcing pattern, based on the observed SST anomalies, was also prescribed in narrow and wider latitude bands (ANOM5 and ANOM30, respectively), and the simulations present differences only in the intensity of the troughs and ridges. From these results we might conclude that the SST anomalies

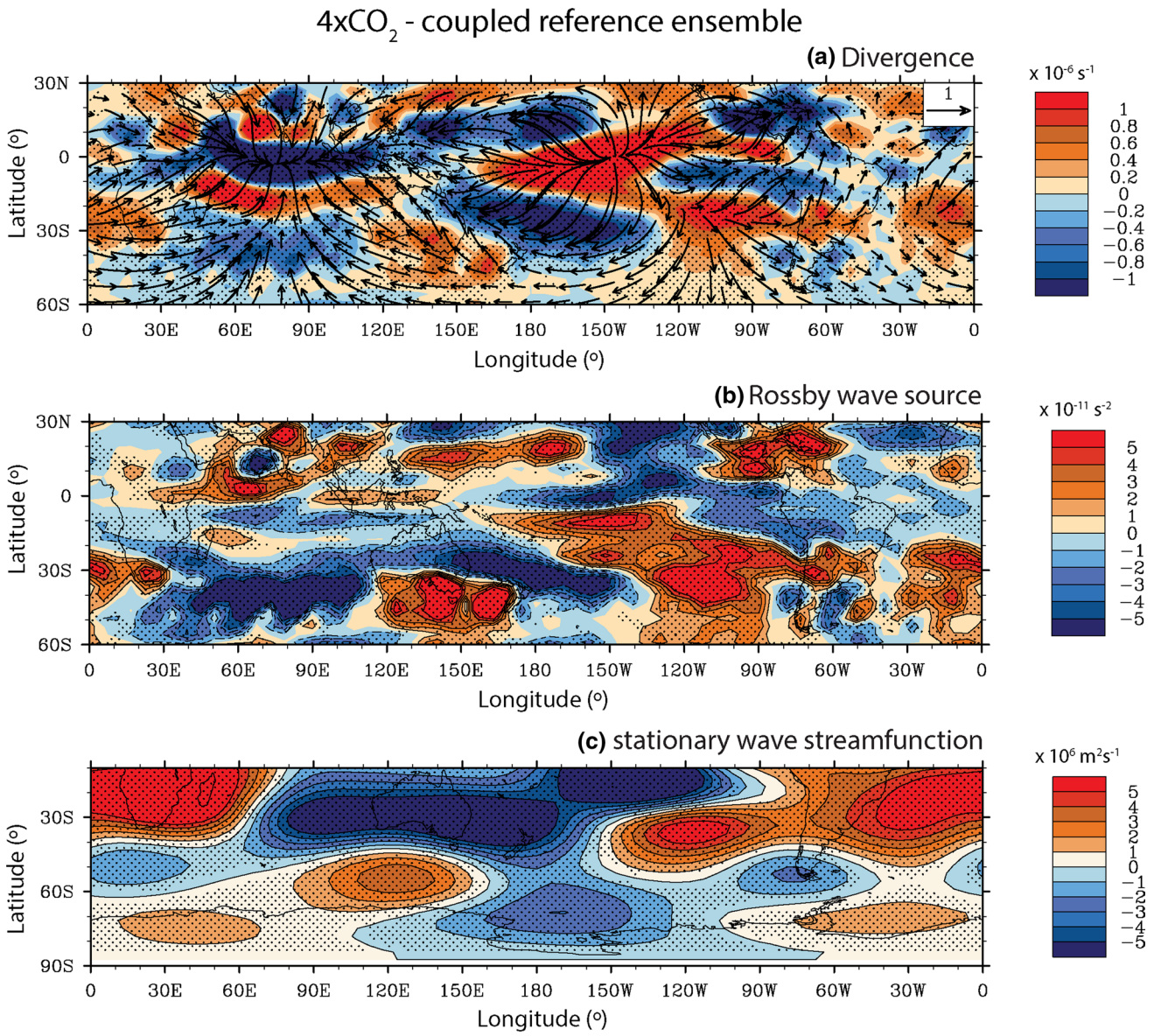

Fig. 16 As for Fig. 15 but for difference between the 4 × CO_2 and coupled-model reference ensemble means

outside the narrow latitude band of 5°S–5°N do not significantly affect the spatial pattern of stationary Rossby wave propagation. To verify this, we average the annual mean SST anomalies from 1871 to 2010, based on the HADISST dataset, in the 5°S–5°N and 30°S–30°N latitude bands. The intensity of the anomalies in the narrow band is much stronger than in the wider band (not shown). This means that only the strongest anomalies found in the 5°S–5°N latitude band could significantly affect the spatial pattern of SRW propagation.

We further examined the combined impact of changes in the strength and width of the HC upon stationary Rossby wave propagation by employing two additional coupled AOGCM simulations with different scenarios of increasing CO_2 concentrations (1 %/year CO_2 and 4 × CO_2). Both simulations showed very similar responses in HC and RWS, namely a HC weakening, a poleward shift of the extratropical boundary, and an upward shift of the HC. However, these responses are much stronger in the 4 × CO_2 simulation, as this scenario represents a dramatic and abrupt change in the radiative forcing.

Comparing the AGCM simulations with the results of AOGCM for two global warming scenarios, some remarkable conclusions can be drawn. Interestingly, the results have shown that the stationary wave streamfunction field for the coupled simulations, in both scenarios, is very similar to what was found in the TH30 atmospheric simulation. In both coupled simulations and in the TH30 atmospheric

simulation, a weakening and a poleward shift of the extratropical boundary of the HC are seen. The weakening of the HC in the TH30 ($4 \times CO_2$) simulation is of the order 3 % (9 %) and the poleward shift of the extratropical boundary is of the order 4 % (3 %). Therefore, although the dominant change in the HC is different between the TH30 and the coupled simulations, the effect upon the stationary Rossby wave propagation is almost the same. This suggests that it is the combined effects of the weakening and the poleward expansion of the HC that determines the changes in stationary Rossby wave propagation. As well, as explained in Sect. 6, it is important to note the role of the indirect radiative forcing due to CO_2 in driving the stationary Rossby wave propagation changes in the TH30 simulation, as the SST is carrying some of the signal of the CO_2 increase. Similar results obtained in the TH30, 1 %/year CO_2 and $4 \times CO_2$ simulations, which represent a warmer climate, also reveal consistency between the coupled and atmospheric simulations. Thus, we can conclude that, in a warmer climate, changes in the strength and width of the HC act together to strongly modify stationary Rossby wave propagation via regional variations in convergence and divergence.

Acknowledgments A.C.V. Freitas acknowledges Fundação de Amparo à Pesquisa do Estado de São Paulo (FAPESP) for financial support (Grant 2012/14231-1) and CSIRO Oceans and Atmosphere for technical support. T.J. O'Kane is supported by an Australian Research Council Future Fellowship (FT120100008). T. Ambrizzi had partial support from CNPq (Grant 300976/2010-0), FAPESP (Grant 2008/58101-9) and VALE Technology Association Institute (ITV-VALE). This work is partly supported by the Australian Government Department of the Environment. We are grateful to Steven Phipps for the assistance with the CSIRO Mk3L model.

References

Caballero R (2007) Role of eddies in the interannual variability of Hadley cell strength. Geophys Res Lett 34:L22705. doi:10.1029/2007GL030971

Caldeira K, Myhrvold NP (2013) Projections of the pace of warming following an abrupt increase in atmospheric carbon dioxide concentration. Environ Res Lett 8:034039

Deser C, Phillips AS (2009) Atmospheric circulation trends, 1950–2000: the relative roles of sea surface temperature forcing and direct atmospheric radiative forcing. J Clim 22:396–413

Franzke CLE, O'Kane TJ, Monselesan DP, Risbey JS, Horenko I (2015) Systematic attribution of observed Southern Hemisphere circulation trends to external forcing and internal variability. Nonlin Processes Geophys 22:513–525

Frederiksen JS, Frederiksen CS (1993) Southern Hemisphere storm tracks, blocking and low-frequency anomalies in a primitive equation model. J Atmos Sci 50:3146–3163

Freitas ACV, Ambrizzi T (2012) Changes in the austral winter Hadley circulation and the impact on stationary Rossby wave propagation. Adv Meteorol 980816:1–15. doi:10.1155/2012/980816

Freitas ACV, Frederiksen JS, Whelan J, O'Kane TJ, Ambrizzi T (2015) Observed and simulated inter-decadal changes in the structure of Southern Hemisphere large-scale circulation. Clim Dyn. doi:10.1007/s00382-015-2519-z

Frierson DMW, Lu J, Chen G (2007) Width of the Hadley cell in simple and comprehensive general circulation models. Geophys Res Lett 34:1–5, L18804. doi:10.1029/2007GL031115

Gabriel CJ, Robock A (2015) Stratospheric geoengineering impacts on El Niño/Southern Oscillation. Atmos Chem Phys 15:11949–11966

Gastineau G, Le Treut H, Li L (2008) Hadley circulation changes under global warming conditions indicated by coupled climate models. Tellus A 60:863–884

Gastineau G, Li L, Le Treut H (2009) The Hadley and Walker circulation changes in global warming conditions described by idealized atmospheric simulations. J Climate 22:3993–4013

Gordon HB, Rotstayn LD, McGregor JL et al (2002) The CSIRO Mk3 climate system model, technical paper 60, CSIRO atmospheric research

Gregory D, Rowntree PR (1990) A mass flux convection scheme with representation of cloud ensemble characteristics and stability-dependent closure. Mon Wea Rev 118:1483–1506

Hoskins BJ, Ambrizzi T (1993) Rossby wave propagation on a realistic longitudinally varying flow. J Atmos Sci 50:1661–1671

Hoskins BJ, Karoly DJ (1981) The steady linear response of a spherical atmosphere to thermal and orographic forcing. J Atmos Sci 38:1179–1196

Hu Y, Fu Q (2007) Observed poleward expansion of the Hadley circulation since 1979. Atmos Chem Phys 7:5229–5236

Johanson CM, Fu Q (2009) Hadley cell widening: model simulations versus observations. J Clim 22:2713–2725

Kanamitsu M, Ebisuzaki W, Woollen J, Yang S-K, Hnilo JJ, Fiorino M, Potter GL (2002) NCEP-DEO AMIP-II reanalysis (R-2). Bull Am Meteorol Soc 83(11):1631–1643

Kang SM, Polvani LM (2011) The interannual relationship between the latitude of the eddy-driven jet and the edge of the Hadley cell. J Clim 24:563–568

Lindzen RS (1994) Climate dynamics and global change. Annu Rev Fluid Mech 26:353–378

Lu J, Vecchi GA, Reichler T (2007) Expansion of the Hadley cell under global warming. Geophys Res Lett 34:L06805. doi:10.1029/2006GL028443

Lu J, Chen G, Frierson DMW (2008) Response of the zonal mean atmospheric circulation to El Niño versus global warming. J Clim 21:5835–5851

Lu J, Deser C, Reichler T (2009) Cause of the widening of the tropical belt since 1958. Geophys Res Lett 36:L03803. doi:10.1029/2008GL036076

Marshall GJ, Connolley WM (2006) Effect of changing Southern Hemisphere winter sea surface temperatures on Southern Annular mode strength. Geophys Res Lett 33:L17717. doi:10.1029/2006GL026627

Müller GV, Ambrizzi T (2007) Teleconnection patterns and Rossby wave propagation associated to generalized frosts over southern South America. Clim Dyn 29(6):633–645. doi:10.1007/s00382-007-0253-x

Müller GV, Berri GJ (2007) Atmospheric circulation associated with persistent generalized frosts in central-southern South America. Mon Weather Rev 135:1268–1289. doi:10.1175/MWR3344.1

O'Kane TJ, Risbey JS, Franzke C, Horenko I, Monselesan DP (2013a) Changes in the metastability of the midlatitude southern hemisphere circulation and the utility of nonstationary cluster analysis and split-flow blocking indices as diagnostic tools. J Atmos Sci 70:824–842

O'Kane TJ, Matear R, Chamberlain M, Risbey J, Sloyan B, Horenko I (2013b) Decadal variability in an OGCM Southern Ocean: intrinsic modes, forced modes and metastable states. Ocean Model 69:121

O'Kane TJ, Risbey JS, Monselesan DP, Horenko I, Franzke CLE (2015) On the dynamics of persistent states and their secular

trends in the waveguides of the Southern Hemisphere troposphere. Clim Dyn. doi:10.1007/s00382-015-2786-8

Oort AH, Yienger JJ (1996) Observed interannual variability in the Hadley circulation and its connection to ENSO. J Clim 9:2751–2767

Phipps SJ (2006) The CSIRO Mk3L climate system model, Technical Report No. 3, Antarctic Climate and Ecosystems Cooperative Research Centre, Hobart, Tasmania, Australia. ISBN 1-921197-03-X

Phipps SJ (2010) The CSIRO Mk3L climate system model v1.2, Technical report No. 4, Antarctic Climate and Ecosystems CRC, Hobart, Tasmania, Australia. ISBN 978-1-921197-04-8

Phipps SJ, Rotstayn LD, Gordon HB, Roberts JL, Hirst AC, Budd WF (2011) The CSIRO Mk3L climate system model version 1.0: part 1—description and evaluation. Geosci Model Dev 4:483–509. doi:10.5194/gmd-4-483-2011

Phipps SJ, McGregor HV, Gergis J, Gallant AJE, Neukom R, Stevenson S, Ackerley D, Brown JR, Fischer MJ, van Ommen TD (2013) Paleoclimate data-model comparison and the role of climate forcings over the past 1500 years. J Clim 26:6915–6936. doi:10.1175/JCLI-D-12-00108.1

Polvani LM, Kushner PJ (2002) Tropospheric response to stratospheric perturbations in a relatively simple general circulation model. Geophys Res Lett 29(7):1–4. doi:10.1029/2001GL014284

Rayner NA, Parker DE, Horton EB, Folland CK, Alexander LV, Rowell DP, Kent EC, Kaplan A (2003) Global analyses of sea surface temperature, sea ice, and night marine air temperature since the late nineteenth century. J Geophys Res 108:1–37

Reichler TJ, Held IM (2005) Evidence for a widening of the Hadley cell. In: 17th AMS conference on climate: Variability and change, American Meteorological Society, Cambridge

Rind D, Perlwitz J (2005) The response of the Hadley circulation to climate changes, past and future. In: Diaz HF, Bradley RS (eds) The hadley circulation: Present, past and future. Kluwer Academic Publishers, Dordrecht, pp 399–435

Robert AJ (1966) The integration of a low order spectral form of the primitive meteorological equations. J Meteorol Soc Japan 44:237–244

Rotstayn LD (1997) A physically based scheme for the treatment of stratiform clouds and precipitation in large-scale models. I: description and evaluation of the microphysical processes. Q J R Meteorol Soc 123:1227–1282

Rotstayn LD (1998) A physically based scheme for the treatment of stratiform clouds and precipitation in large-scale models. II: comparison of modelled and observed climatological fields. Q J R Meteorol Soc 124:389–415

Rotstayn LD (2000) On the "tuning" of autoconversion parameterizations in climate models. J Geophys Res 105:15495–15507

Sardeshmukh PD, Hoskins BJ (1988) The generation of global rotational flow by steady idealized tropical divergence. J Atmos Sci 45:1228–1251

Seidel DJ, Fu Q, Randel WJ, Reichler TJ (2008) Widening of the tropical belt in a changing climate. Nat Geosci 1:21–24

Shimizu MH, Cavalcanti IFA (2011) Variability patterns of Rossby wave source. Clim Dyn 37:441–454

Tandon NF, Gerber EP, Sobel AH, Polvani LM (2013) Understanding Hadley cell expansion versus contraction: insights from simplified models and implications for recent observations. J Clim 26:4304–4321

Taschetto AS, Ambrizzi T (2012) Can Indian Ocean SST anomalies influence South American rainfall? Clim Dyn 38(7):1615–1628. doi:10.1007/s00382-011-1165-3

Tyrrell GC, Karoly DJ (1996) Links between tropical convection and variations of the extratropical circulation during TOGA COARE. J Atmos Sci 53(18):2735–2748

Vidyunmala V, Nanjundiah RS, Srinivasan J (2007) The effect of variation in sea-surface temperature and its meridional gradient on the equatorial and off-equatorial ITCZ in an aquaplanet general circulation model. Meteorol Atmos Phys 95:239–253

Wang W-C, Liang X-Z, Dudek MP, Pollard D, Thompson SL (1995) Atmospheric ozone as a climate gas. Atmos Res 37:247–256